



HAL
open science

Study and Simulation of Low Energy Plasma Measurement on Solar Orbiter

S. Guillemant, J.C. Matéo-Vélez, V. Genot, P. Sarrailh, A. Hilgers, P. Louarn

► **To cite this version:**

S. Guillemant, J.C. Matéo-Vélez, V. Genot, P. Sarrailh, A. Hilgers, et al.. Study and Simulation of Low Energy Plasma Measurement on Solar Orbiter. Spacecraft Charging Technology Conference 2014 (13th SCTC), Jun 2014, PASADENA, United States. hal-01081360

HAL Id: hal-01081360

<https://hal.science/hal-01081360>

Submitted on 7 Nov 2014

HAL is a multi-disciplinary open access archive for the deposit and dissemination of scientific research documents, whether they are published or not. The documents may come from teaching and research institutions in France or abroad, or from public or private research centers.

L'archive ouverte pluridisciplinaire **HAL**, est destinée au dépôt et à la diffusion de documents scientifiques de niveau recherche, publiés ou non, émanant des établissements d'enseignement et de recherche français ou étrangers, des laboratoires publics ou privés.

(Abstract No 148)

Study and Simulation of Low Energy Plasma Measurement on Solar Orbiter

S. Guillemant, J.-C. Matéo-Vélez, V. Génot, P. Sarrailh, A. Hilgers, Ph. Louarn

Abstract—The flux of particles collected by scientific low energy detectors are sensitive to absolute and differential potentials, and may include both ambient and secondary particles emitted by the spacecraft itself. This work presents numerical models of particle detector behaviour on Solar Orbiter, using the SPIS software. The results presented in this paper show the necessity to take into account the spacecraft plasma interactions at the earlier stage of scientific missions' definition, as well as during measurement interpretation. It demonstrates that electrons emitted in the vicinity of the detectors may be the main contributor to low energy electron measurements pollution.

Keywords—low energy plasma; particle detectors; numerical modelling; secondary emission

I. INTRODUCTION

Scientific missions dealing with low energy space plasma measurements are subject to the effects of spacecraft charging and interactions with the environment. These interactions also involve the detector itself and include ambient particle deflection, acceleration or deceleration, emission of particles from the spacecraft and recollection by the instrument. It may lead to erroneous interpretations of measurements pending on the detector location, spacecraft geometry and materials and ambient conditions. In previous works, it was shown that a spacecraft submitted to the solar wind will charge positive between 1 AU and 0.1 AU, due to the dominant photoemission process. Below 0.1 AU however, the charging is negative due to the strong recollection of photoelectrons and secondary electrons due to electron impact, which is induced by space charge barriers of potentials ([1]-[2]). Strong detector perturbations are expected.

ESA planned missions dealing with low energy plasma measurements involve Solar Orbiter (SOLO) and JUICE. They must measure solar wind plasma characteristics, typically ranging from below 1 eV up to 100 eV in energy, 1 to 100 particles per cubic meter and drift velocity from 100 to 400 km/s. The interaction with magnetospheres is also an objective. Electrostatic cleanliness becomes a key issue. The objective of this paper is to illustrate the importance of spacecraft plasma interaction, to propose means to anticipate disturbance and to

investigate how measurements can be better understood (and possibly corrected). For a complete list of possible spacecraft plasma interaction, the reader may refer for instance to [3]. In this paper we focus on Solar Orbiter and on its electron analysers.

The difficulty of predicting and understanding detectors measurements relies on the following aspects. First, the spacecraft globally floats to a non-null potential and deflects charge carriers, especially at low energy. Spacecraft shapes and differential charging complicates the particles trajectories, which may be far from a spherical symmetry model. The interaction with the spacecraft generates secondary particles, mainly due to ambient electron and photon impacts. The yields strongly depend on materials. In addition, material properties (conductivity, yields) depend on the temperature and sometimes on the impacting fluxes. Finally, one may expect space charge effects in the plasma, due to large secondary electron densities in the vicinity of the spacecraft, but also to wake effects for supersonic ions.

In this work we propose first a comparison between a classical analytical method (based on Liouville's theorem) and a self-consistent 3D numerical approach taking into account only the detector geometry. Both methods are used to calculate the measured distribution function as a function of the detector potential, both for ambient and secondary electrons emitted by the detector itself. In a second part, the SOLO spacecraft is simulated with its Electron Analyzer System (EAS). Global and differential charging effects are assessed at spacecraft and at detector levels.

II. MODELLING LOW ENERGY PARTICLE DETECTORS

The principle of electron measurement on SOLO is described in section A. Section B presents the analytical theory used to interpret ambient electron measurements. Section C is a numerical model permitting to assess the level of confidence of the analytical model, and to raise the question of secondary electrons.

A. Measurement Principle

SOLA EAS represented in Fig. 1 is a top-hat electrostatic analyser. Fig. 2 is a schematic view of its design. Biased plates are mounted just behind the aperture grids and are used to deflect the particle trajectories. The analyser field of view (FOV) is $\pm 45^\circ$. It allows overcoming the limited field of view of simple hemispherical electrostatic analyser. Combined with a spinning satellite body or a second particle detector on the opposite side, the instrument configuration can easily provide

S. Guillemant, J.-C. Matéo-Vélez and P. Sarrailh are with ONERA - The French Aerospace Lab, Toulouse, France (e-mail: Mateo@onera.fr)

S. Guillemant, V. Génot and Ph. Louarn are with the Institut de Recherche en Astrophysique et Planétologie, Toulouse, France (e-mail: sStanislas.Guillemant@irap.omp.eu).

A. Hilgers is with the European Space Agency / ESTEC, Noordwijk, The Netherlands (e-mail: Alain.Hilgers@esa.int)

(Abstract No 148)

coverage of the entire 4π steradians of the particle environment. The EAS analyser mounted on three axis stabilized Solar Orbiter spacecraft is a set of two such sensors, which covers the entire surrounding electron environment. Electrons entering the system are deflected by the internal set of curved electrodes, pending on their potentials, and finally collected on micro channel plate detector (MCP). The signal collected is the results of two processes. First, the deviation of the particle flux in the gaseous phase is denoted by the transformation of the undisturbed velocity distribution function, denoted as f_∞ , into a distribution f_D at the detector grid entrance. In this work, we focus on this first transformation only. The assessment of the internal deflection and effective geometrical factor, leading from f_D to the measured distribution f_M , is generally performed by experimental calibration and/or specific numerical modelling [4]. This latter part is not treated in the present paper.



Fig. 1. Electrostatic analyser SWA-EAS for Solar Orbiter [source: D.O. Kataria and C. Owen from MSSSL].

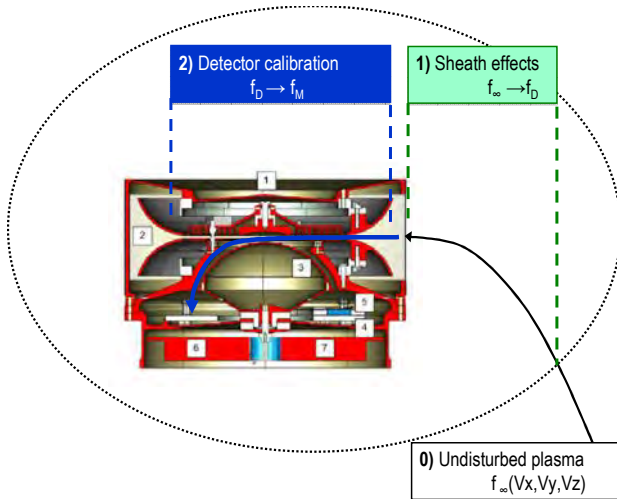


Fig. 2. Top-hat measurement principle.

B. Analytical Estimation of the Distribution Function

The first approach used to estimate the transformation of f_∞ into f_D relies on the Liouville's theorem, which states that the value of the velocity distribution function is conserved in phase space along a trajectory. Assuming 1/ an isotropic velocity distribution f_∞ , 2/ all trajectories at detector entrance are filled (i.e. come from the undisturbed plasma and not from the detector or spacecraft), 3/ collisionless plasma; we conclude that for any velocity V_d on the detector corresponding to V_∞ , at infinite:

$$f_D(V_D) = f_\infty(V_\infty) \tag{1}$$

In addition, total energy conservation of the particle writes:

$$V_D = \sqrt{V_\infty^2 - \frac{2q\phi_D}{m}} \tag{2}$$

where q is the electrical charge unit, ϕ_D the detector entrance grid potential and m the particle mass. Finally, we must get rid of particles which have a negative total energy on the detector. The result of this classical analytical approach is represented in Fig. 3, assuming f_∞ is a maxwellian electron distribution of temperature 10 eV and density 10^6 m^{-3} represented by the energy and velocity distribution (blue curves) of Fig. 3. The data illustrates the change due to a biased detector at $\pm 10 \text{ V}$. The velocity distribution function is shifted following Liouville's theorem. The change in the energy distribution function is a bit more complex, and is not a simple shift.

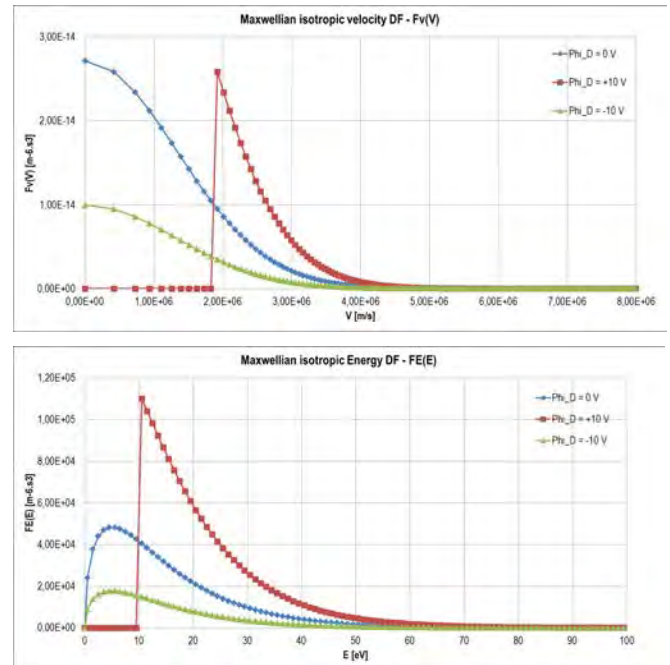


Fig. 3. Differential velocity and energy distributions obtained at detector entrance, for null, positive and negative potentials

(Abstract No 148)

This approach is similar to and provides the same results as [6]. The Boltzmann attenuation factor is obtained in the case of a repulsive object (green curve in Fig. 3). For an attractive detector, it results in a shifted and amplified signal (red curve). This latter curve provides exactly the Orbit Motion Limited (OML) integrated current.

C. Numerical modelling

A numerical approach is used to compare with the above theoretical analysis. It consists in simulating the electron collection by two planar surfaces located on a cylindrical-shape instrument, see Fig. 4. SPIS, the Spacecraft Plasma Interaction Software, is used to simulate 1/ plasma dynamics around the object, 2/ plasma interaction with object surfaces, 3/ measurements of distribution functions [5]. The first two points relies on the inherited software capabilities. The latter point has been significantly improved in the last version of the code (version 5). The numerical method behind is described in a companion paper [8]. The algorithm permits to refine the statistics on the (small) instrument surface, to refine smoothly the three-velocity distribution function in the relevant energy domain.

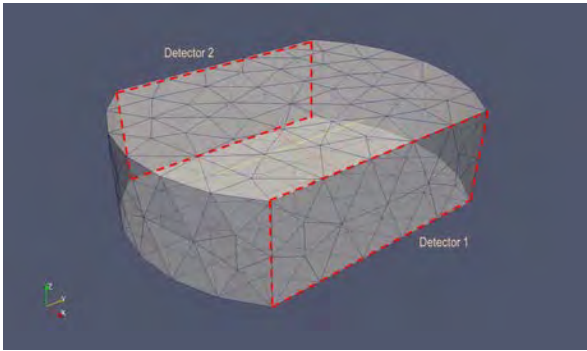


Fig. 4. Geometry of the numerical instrument

Simulation ID	SOLO@0.28 AU
Distance (AU)	0.28
Distance (R_s)	60.2
Sun Flux (# 1AU)	12.76
Elec. density N_e (m^{-3})	1.04×10^8
Elec. temp. kT_e (eV)	21.37
Ion density N_i (m^{-3})	1.04×10^8
Ion temp. kT_i (eV)	27.0

Fig. 5. Typical plasma characteristics at 0.28 AU

The instrument is immersed in a maxwellian plasma representative of the solar wind at 0.28 AU, see Fig. 5. In the present case, no plasma drift is simulated in order to be consistent with the analytical model. The cylinder is 7 cm in diameter and 2 cm in height. Each detecting surface is 5 cm by 2 cm. Detectors 1 and 2 face the +X and -X directions respectively. The instrument is located within a spherical simulation box of radius 5 m. The mesh grid size is 70 cm at the external boundary and 1 cm at the instrument. The instrument is covered with conductive Indium Tin Oxide (ITO). The sun flux is directed towards -X (detector 2 is not

illuminated hence), with a small fraction in the -Z direction, signifying that the top flat surface in Fig. 4 is slightly illuminated. The secondary electron yield is represented in Fig. 6. Only the very beginning of the curve, for primary electron energy lower than 100 eV is of interest.

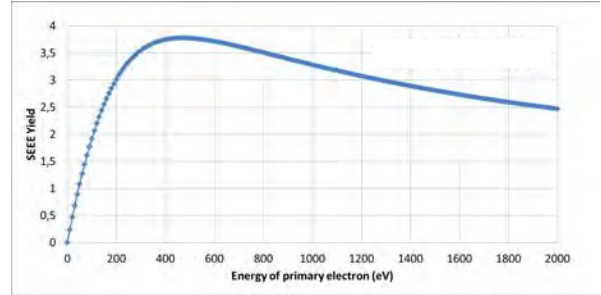


Fig. 6. Secondary electron emission yield under electron impact for ITO, assuming isotropic primary electron flux

The ambient electron distribution measured by the numerical instrument, *i.e.* the sum of detector 1 and 2, is compared to the injected distribution function when the instrument potential is null in Fig. 7.

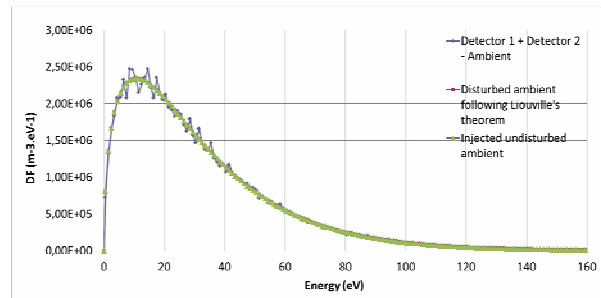


Fig. 7. Measured numerical distribution (blue line) in comparison to undisturbed distribution (green line), with null instrument potential.

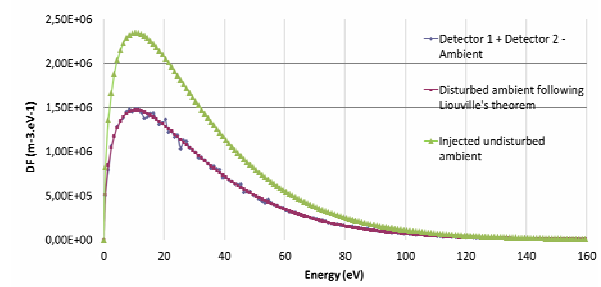


Fig. 8. Measured numerical distribution (blue line) in comparison to undisturbed distribution (green line), and to analytical distribution (red line), with repulsive instrument potential of -10 V.

(Abstract No 148)

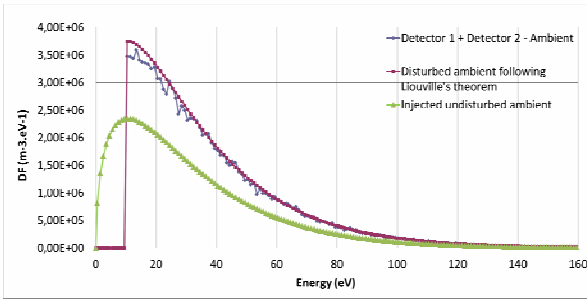


Fig. 9. Measured numerical distribution (blue line) in comparison to undisturbed distribution (green line), and to analytical distribution (red line), with attractive instrument potential of +10 V.

The repulsive case is also well reproduced by the simulation in Fig. 8. The attractive case of Fig. 9 qualitatively agrees with the analytical OML model, except at low electron energy, around 10 to 30 eV. This is explained by the fact that the instrument is not spherical. In this case, electrons emitted in backtracking with a grazing incidence are recollected by the instrument itself before reaching back the simulation box external boundary. Associated with low energy, these grazing incidence angle are only filled by electron coming from the instrument itself (secondary electrons). Integrating the distribution functions leads to a discrepancy of 3 % between the two methods.

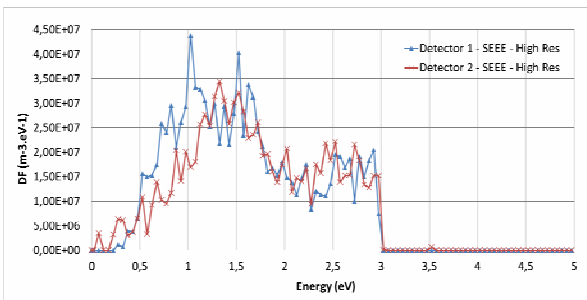


Fig. 10. Measured SEEE distribution with an attractive instrument potential of +3 V. Blue curve is detector 1. Red curve is detector 2.

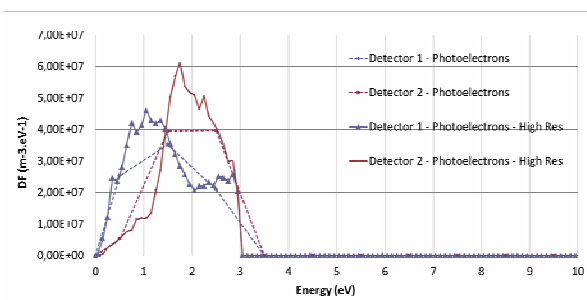


Fig. 11. Measured photoelectron distribution with an attractive instrument potential of +3 V. Blue curve is detector 1. Red curve is detector 2.

Detection of secondary electrons emitted by primary electron impact (SEEE) is a matter of secondary electron energy. When the instrument is negative, no such electron is

recollected. The plot of Fig. 10 was obtained for a potential of +3 V on the instrument. No electron of energy larger than 3 eV is recollected. They have all enough energy to get emitted definitely to the undisturbed plasma. Both detectors provide the same result. This is not the case when detecting photoelectrons, see Fig. 11. The origin of the energy peak difference is related to the asymmetry of the photoelectron emission surfaces. In Fig. 12, detector 1 faces the Sun. The positive potential of +3 V attracts very low energy electrons efficiently. Electrons of less than 1 eV are collected locally. On the contrary electrons of 2 eV can travel a larger distance and be collected somewhere else on the instrument. This is why the instrument 2 collects larger energy electrons, which can extend further from the instrument before being re-attracted toward the instrument. This illustrates very well that even shaded detector surface may collect photoelectrons.

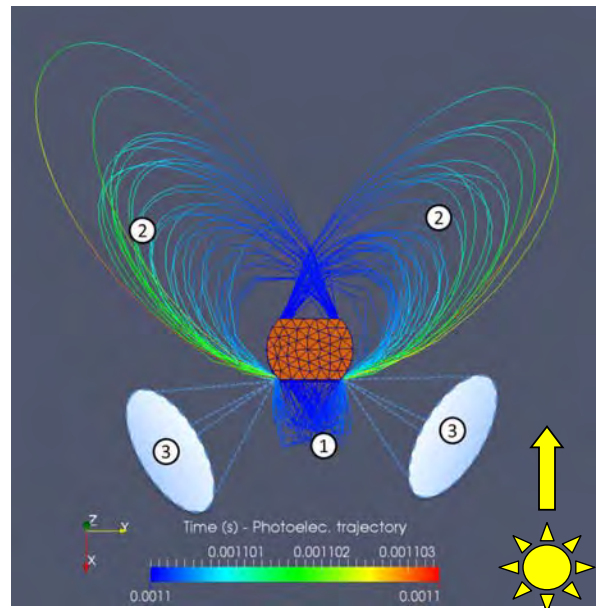


Fig. 12. Photoelectron trajectories when instrument potential is +3 V

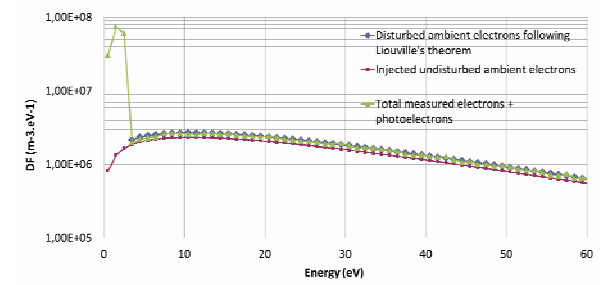


Fig. 13. Total differential energy flux of electrons.

To sum up, this part suggests that there is a good agreement between analytical and numerical results in case of negative potentials, with no pollution by secondary particles. In case of positive potential, some ambient electron trajectories with grazing incidence angles are intercepted by the detector itself, which decreases the detection efficiency for ambient particles.

(Abstract No 148)

The pollution by secondary particles is large as seen in Fig. 13, which sums the contributions of all electrons (primary, secondary) for a potential of +3 V. The energy cut-off to be applied to such an ambient electron instrument seems to be 3 eV, *i.e.* the spacecraft (positive) potential. The next part will show however that this simplistic result is not applicable to realistic spacecraft configurations equipped with an instrument.

III. MEASUREMENTS ON SOLAR ORBITER

Section A describes the SOLO mission and section B the numerical model used to estimate its behaviour at 0.28 AU. Section C presents the result of the spacecraft plasma interaction, in terms of field and matter. Section D finally shows the impact of this specific equilibrium state onto electron measurement.

A. Mission description

The ESA Solar Orbiter mission scheduled for a launch in 2017-2018, is dedicated to solar and heliospheric physics. It has been selected within the ESA Cosmic Vision Programme 2015-2025. Solar Orbiter will study, through a combination of in-situ and remote sensing observations the heliosphere and its magnetic field, the solar wind and solar energetic particles among other phenomena. It will provide close-up, high-latitude observations of the Sun. Solar Orbiter will have a highly elliptic orbit: between 0.9AU at aphelion and 0.28AU at perihelion.

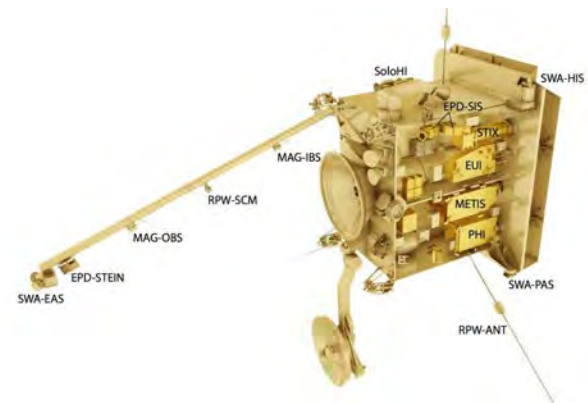


Fig. 14. Payload accommodation on-board Solar Orbiter. Credit: ESA

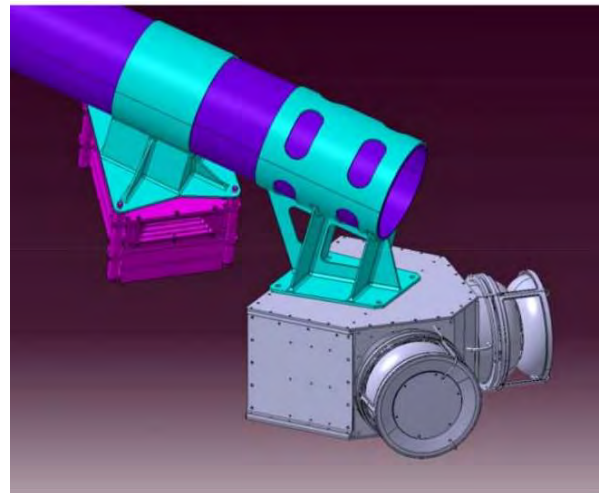


Fig. 15. SWA/EAS CAD model. Source: SWA/EAS Instrument Design Report.

The SOLO structure design projected by ESA is illustrated in Fig. 14 (note that now the geometric configuration and the dimensions have low probabilities of changing in the near future). It is composed of a spacecraft body of dimensions $1.70 \times 1.70 \times 1.80$ m, a sunshield of $2.50 \times 2.50 \times 0.09$ m, two solar panels of $3.80 \times 1.20 \times 0.02$ m, a high gain antenna (HGA) 0.50 m in radius and 0.02 m in depth, three radio and plasma waves experiments antennas (RPW) 5.30 m in length and 0.006 m in radius, a rear boom of length 4 m and 0.02 m in radius, at the end of which the electron analyser EAS is located, see Fig. 15. EAS dimensions are $0.20 \times 0.18 \times 0.11$ m.

B. Numerical Modelling

The CAD geometry simulated with Gmsh [7] is represented in Fig. 16. The main elements described in section A are meshed using meshed surfaces, except RPW antenna which are modelled by thin wires, *i.e.* without a thickness. It permits to save mesh grid cells by avoiding very small cells as compared to other spacecraft surfaces. The EAS device is modelled by a metallic case and two instruments, each one composed of 8 detecting surfaces (as those defined in Fig. 4). The spacecraft plasma interaction is modelled using SPIS, in an ovoid domain of radius around 40 m, see Fig. 17. The mesh grid size extends from 0.005 m on the EAS detector of Fig. 18 to 1.5 m at the outer boundary, for a total number of tetrahedron cells of 270,000. Thin wires modelling described in the companion paper proposes a cylindrical approach for the electric field (potential follows a $\ln(r)$ law) [8]. Particle collection and secondary emission is calculated.

(Abstract No 148)

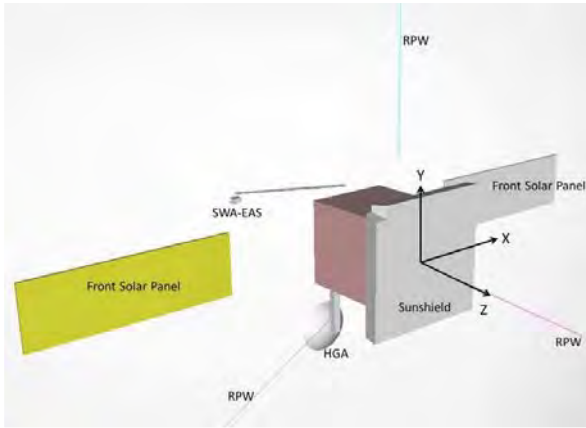


Fig. 16. CAD geometry of SOLO

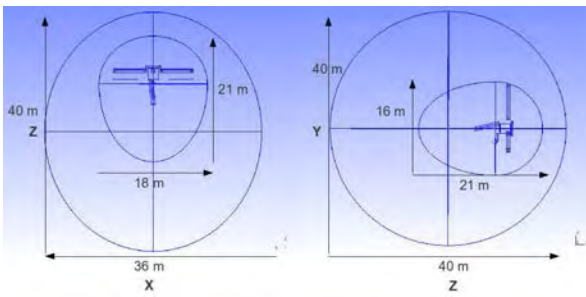


Fig. 17. Spacecraft geometry inside the simulation box. An intermediate and virtual ovoid box is used to force a progressive mesh refinement close to the spacecraft.

Materials used on the spacecraft are described in Fig. 19. CFRP is used on the sun shield, HGA support, rear boom and solar array rear faces. Black kapton is used on the spacecraft body. CERS cover glass material is used on the sunlit side of the solar arrays. HGA is composed of aluminium oxide and the RPW antenna of gold. Steel composes the EAS box at the exception of the grid entrance which is assumed not to emit particles (material is "Steel for detectors").

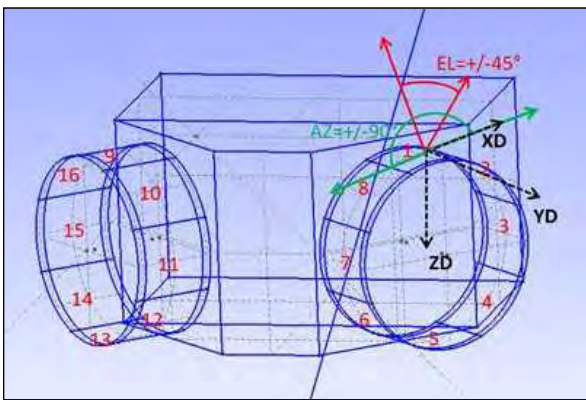


Fig. 18. Definition of 16 detecting surfaces on the EAS numerical model

Characteristics	Material							
		CFRP	Black Kapton	CERS	Steel	Steel for detectors	AlOx for HGA	Gold
BUC	Bulk conductivity (ohm.m)	N/A	N/A	9.99E-15	N/A	N/A	1.00E-12	N/A
PEE	Primary elec Energy for max SEEY(keV)	0.30	0.15	0.80	0.25	0.25	0.35	0.80
IPE	Proton energy for max SEEP yield (keV)	135	140	230	140	140	230	135
SRE	Surface resistivity (ohm)	N/A	N/A	9.99E14	N/A	N/A	N/A	N/A
PEY	Photoelectron current at 1AU (A/m2)	7.19E-6	4.99E-6	1.99E-5	1.99E-5	0.00	3.99E-5	2.90E-5
RPR1	Range parameter r1 (Angstrom)	110	71.48	70	70	70	50	88.79
RPR2	Range parameter r2 (Angstrom)	300	312.10	150	150	150	100	53.47
MSEY	Max SEEY	0.69	2.09	5.50	2.50	0.00	3.50	1.29
SEY	SEEY due to impact of 1keV protons	0.41	0.45	0.24	0.45	0.00	0.24	0.41
RPN1	Range parameter n1	1.89	0.60	0.50	0.60	0.60	0.60	0.92
RPN2	Range parameter n2	1.03	1.76	1.64	1.79	1.79	1.64	1.73
RDC	Relative dielectric constant	1.00	3.50	3.79	1.00	1.00	10.00	1.00
Thick.	Material thickness (m)	1.25E-4	1.25E-4	1.25E-4	1.25E-4	1.25E-4	1.25E-4	1.25E-4

Fig. 19. Material electrical properties

The environment considered here is the same as in part II, except that protons have a drift velocity of 400 km/s in the -Z direction, which is also the direction of the Sun flux. The ambient plasma Debye length is 3.4 m. A full PIC approach is used to model plasma dynamics, composed of ambient electron and protons, and of secondary electrons emitted by electron, proton and photon impact. The photoelectron fluxes at normal incidence presented Fig. 19 are multiplied by 12.8 to take account of the amplified Sun flux at 0.28 AU, in comparison to the values given at 1 AU. Photoelectron and SEEE electron distribution are maxwellian with a temperature of 3 and 2 eV respectively. The external boundary condition assumes a $1/r^2$ potential evolution, relevant for plasma pre-sheath regions. The number of numerical super particles is 3.5×10^6 , 1.5×10^6 , 1.4×10^6 , 2.5×10^6 and 0.6×10^6 respectively for ambient electrons, ambient protons, photoelectrons, SEEE and SEEP electrons (where SEEP stands for secondary electrons from proton impact).

C. Spacecraft plasma interaction

The equilibrium spacecraft potential, reached buy all conductive surfaces is +3 V. Note this is the same potential as used in Part II.C. The solar array sunlit face is floating at +14 V due to photoelectron emission and large SEEE yield. The HGA is floating at + 9V due to its large SEEE yield. The plasma potential map is presented in Fig. 20 and in Fig. 21. A non-monotonous potential is observed in the sunlit and wake direction. At the front face, the -1.25 V potential is the result of a strong negative space charge due to photoelectrons, which is consistent with previous results using a simplified geometry [1]. On the rear side, a negative potential region of -2.75 V is obtained due to proton deflection and presence of secondary electrons. The wake extends far from the spacecraft due to the large proton Mach number of 8. Of particular interest is the

(Abstract No 148)

sharp decrease of potential close to the EAS position at $Z = -6$ m in Fig. 21, where we obtain a negative potential difference of approximately -3 V when looking towards the spacecraft and of -6 V when looking in the opposite direction.

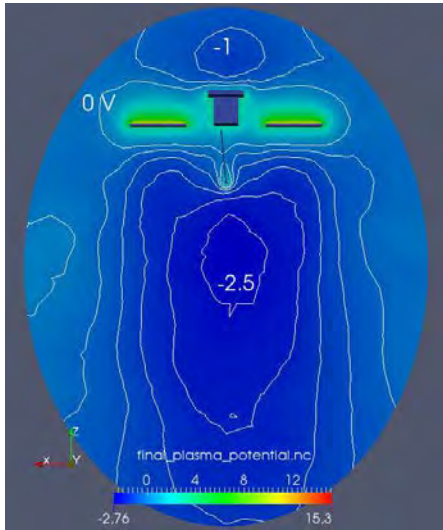


Fig. 20. Plasma potential around SOLO at 0.28 AU

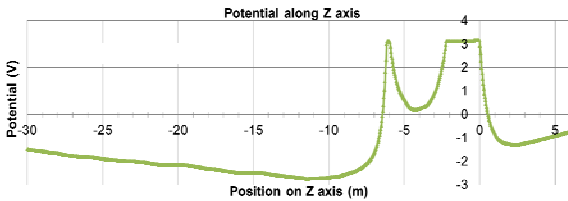


Fig. 21. Potential profile along the Z-axis passing through the middle of the spacecraft.

The proton wake is depicted in Fig. 22. It extends over the full box size. The solar panels, the spacecraft hub and the HGA are the main source of proton depletion. Maxwellian ambient electrons are almost not affected by the spacecraft potential due to their large temperature of 22 eV, and have a uniform density of $1 \times 10^8 \text{ m}^{-3}$. Photoelectron density is maximal in the vicinity of sunlit surfaces and reaches $5 \times 10^9 \text{ m}^{-3}$, which is at least one order of magnitude larger than ambient plasma. Due to spacecraft positive potential, photoelectrons spread out and then are recollected, even on the wake side. In the vicinity of the EAS instrument however, the density is quite small, lower than $1 \times 10^7 \text{ m}^{-3}$. Secondary electron emission under electron impact being isotropic, the density is very homogeneous close to spacecraft surfaces, including the EAS vicinity. The recollection of these secondaries is efficient since they have a temperature (2 eV) of the same order of the negative potential barriers around spacecraft surfaces.

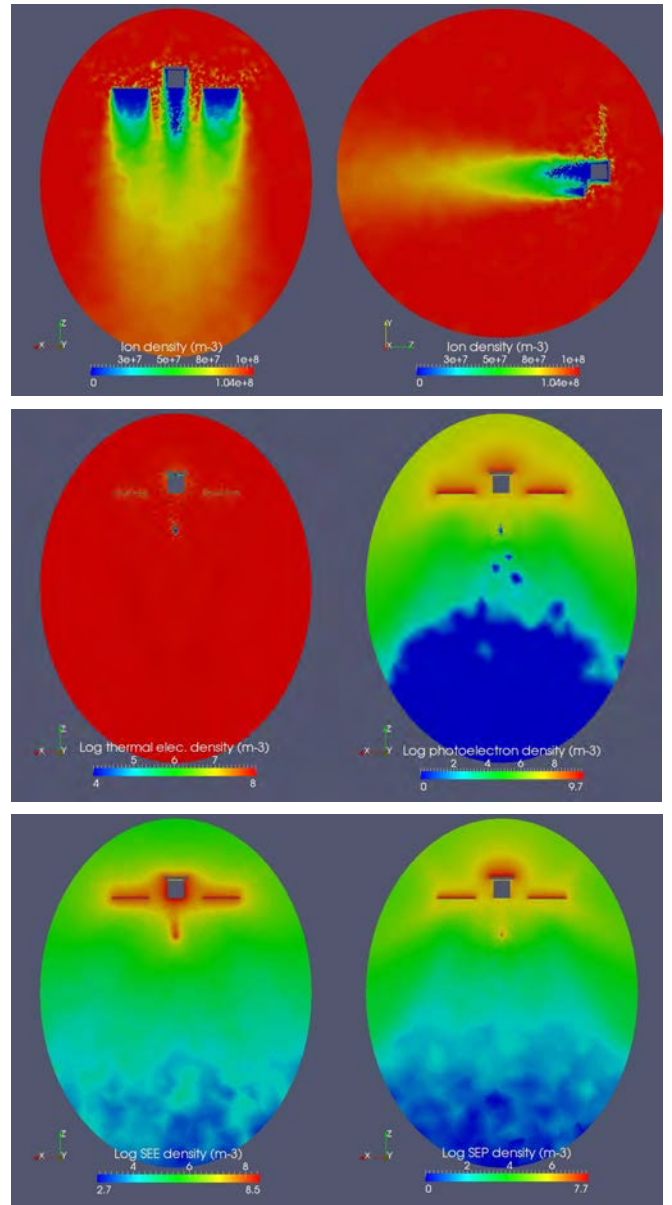


Fig. 22. Density of ion (top plots), ambient electron and photoelectron (middle plots, log scale), secondary electron under electron and proton impact (bottom plots, log scale).

D. Electron Measurements

Spacecraft charging and plasma sheath structure have a deep impact on electron detection by EAS, even if it is located at the end of a long boom. EAS does collect secondaries which could be interpreted as ambient electrons. Ambient electrons themselves are necessarily deflected by the spacecraft potential, which also intercept electron that would have been collected by the instrument. This complexity adds to the basic situation reported in part II.

The ambient electron perturbation is presented in Fig. 23 which compare the energy distribution measured by the 16 sensors (blue curve), with the injected maxwellian distribution (green curve). The theoretical distribution obtained by

(Abstract No 148)

analytical modelling (red curve) is very different from the simulated data. There is a lack of detection on the low energy range. First, the detection starts at 5 eV instead of 3 eV as expected from the results obtained in Part II. This is explained by the presence of negative barriers of potentials around the EAS box that prevent very low energy ambient electron to reach the instrument. Second, there is a global decrease of the flux, even for large energies. This is mainly due to the interception of a fraction of the flux by spacecraft hub and solar arrays. Integrating the distribution functions we get a discrepancy of 13 % between the measured and analytical data. The analytical model is thus only approximate. Reversing the measured distribution into the undisturbed plasma is something difficult to do and numerical simulation helps avoiding some trips.

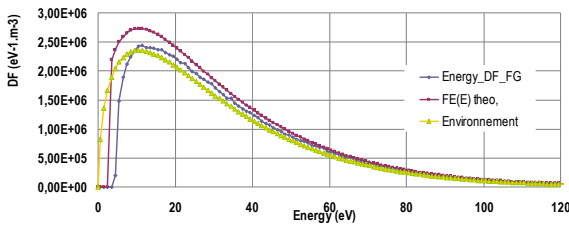


Fig. 23. Measured ambient electron

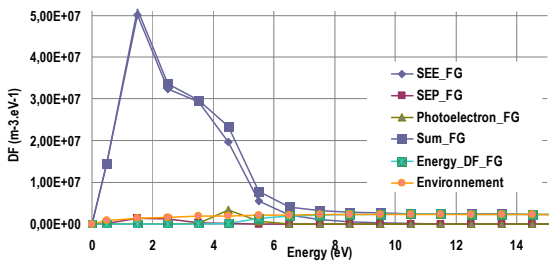


Fig. 24. All electron populations energy distributions

The perturbation of the low energy channels of the instruments is clear on Fig. 24. The main source is the SEEE, which completely overpass other currents in the low energy range. Photoemission is negligible. Part II concluded that the measured energy distribution is not relevant for energies lower than the spacecraft attractive potential of 3 V. Here, we see that the perturbation occurs at energies up to 10 eV. This is due to the impingement of secondaries emitted by surfaces close to the instrument entrance grids, especially the EAS instrument ground case itself. Some of them are in direct view of the slits and provide a large amount of measurement contamination, as seen on the trajectory plots of Fig. 25. Ambient electrons are quite efficiently deflected. Photoelectrons come from the sunshield and from the RPW antennas. No such electron come from the solar arrays because their positive potential prevents them from escaping and makes them recaptured very locally. Finally, the origin of the SEEE pollution is the detector itself.

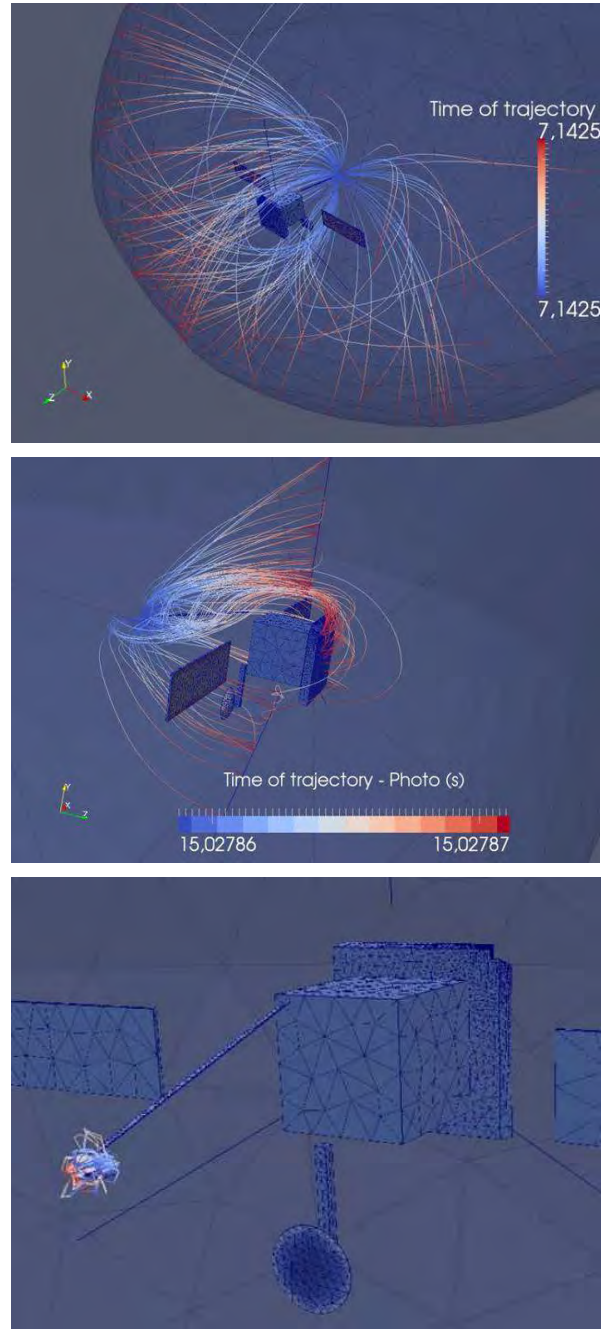


Fig. 25. Trajectories of electrons collected by the instrument. Top: ambient. Middle: Photoelectrons. Bottom: SEEE.

IV. CONCLUSION

This paper shows that understanding spacecraft charging and interaction with the plasma is of prime importance for a precise analysis of particle instruments, especially at low energy. In a first part, we showed that analytical and numerical models can provide rather good estimation of the detection made by a detector virtually let alone in the environment. However, the attractive case leads to some percents errors due to instrument geometrical effects that prevent some particles to

(Abstract No 148)

be actually collected by the non-spherical instrument. In a second step, it was demonstrated that locating the detector on a real spacecraft in realistic situations increase the discrepancy between the simple analytical model and the more adapted numerical approach. The deflection of electrons by the spacecraft and their interception before collection produced a loss of around 10 %. The error made is much larger when looking at secondary particles, whose origin is the detector itself or its neighbouring components.

ACKNOWLEDGMENT

This work was supported partly by ESA in the frame of the SPIS-SCIENCE Contract No. ESTEC/4000102091/10/NL/AS, and partly by CNES and French Région Midi-Pyrénées in the frame of PhD funding.

REFERENCES

- [1] S. Guillemant, V. Génot, J.-C. Mateo Velez, P. Sarrailh, A. Hilgers, P. Louarn, Simulation Study of Spacecraft Electrostatic Sheath Changes With the Heliocentric Distances from 0.044 to 1 AU, *Transactions on Plasma Science*, vol. 41, No 12, pp. 3338-3348, 2013.
- [2] S. Guillemant, V. Genot, J.-C. Mateo-Velez, R. Ergun, and P. Louarn, Solar wind plasma interaction with solar probe plus spacecraft, *Ann. Geophys.*, 30, 1–18, 2012 -- www.ann-geophys.net/30/1/2012/ -- doi:10.5194/angeo-30-1-2012.
- [3] S. Lai, *Fundamentals of Spacecraft Charging: Spacecraft Interactions with Space Plasmas*, Princeton University Press, 2012.
- [4] G. A. Collinson et al., The geometric factor of electrostatic plasma analyzers: A case study from the Fast Plasma Investigation for the Magnetospheric Multiscale mission, *Rev. Sci. Instrum.* 83, 033303 (2012); <http://dx.doi.org/10.1063/1.3687021>
- [5] www.spis.org
- [6] Laframboise J. G. and Parker L. W. Probe design for orbitlimited current collection. *The Physics of Fluids*, Vol. 16, N. 5, 1973.
- [7] <http://geuz.org/gmsh/>
- [8] P. Sarrailh, J.-C. Matéo-Vélez, S. Hess, J.-F. Roussel, B. Thiébault, J. Forest, B. Jeanty-Ruard, A. Hilgers, D. Rodgers, F. Cipriani, SPIS 5: new modelling capabilities and method for scientific mission, this issue.

Electrostatic cleanliness effect on low energy plasma measurement

Application on Solar Orbiter case

S. Guillemant^(1,2), J.-C. Matéo-Vélez⁽¹⁾, V. Génot⁽²⁾, P. Sarrailh⁽¹⁾
A. Hilgers⁽³⁾, Ph. Louarn⁽²⁾

13th SCTC, Pasadena, CA, USA, 23-27/06/2014

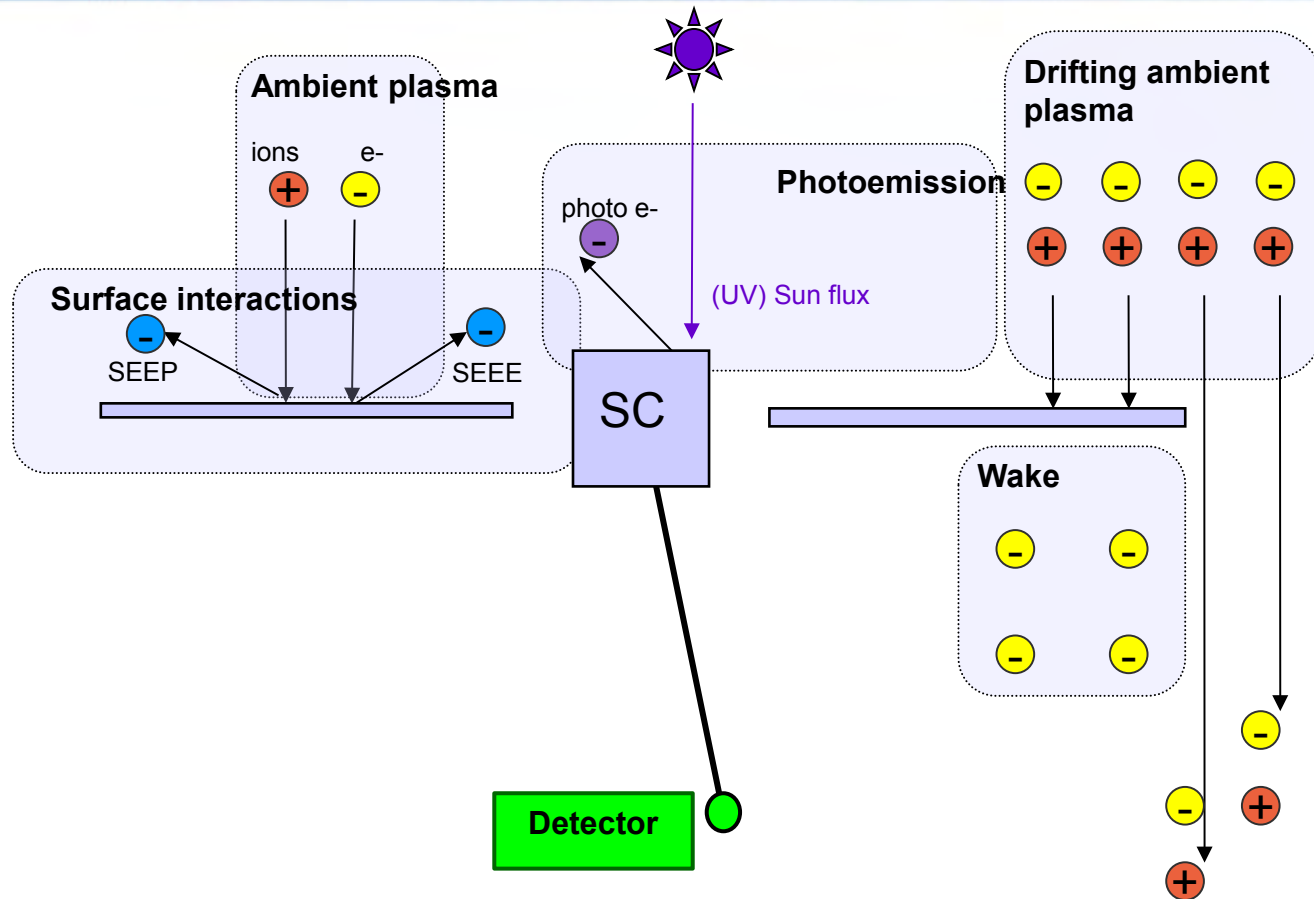


r e t u r n o n i n n o v a t i o n

Context

- Scientific context
 - ESA planned missions dealing with low energy plasma measurements: Solar Orbiter, JUICE
 - Solar wind in short: 10-100 eV, 1-100 #/cm³, 100 – 400 km/s
 - Interaction with planet magnetospheres
 - Electrostatic cleanliness becomes a key issue
- Objectives of this presentation
 - To illustrate the importance of spacecraft plasma interaction
 - To highlight the disturbance from secondary electrons
- Method
 - Model the detector alone
 - Model the detector + the spacecraft

Spacecraft Plasma Interaction and Detection



Many questions / uncertainties for particle detection

What does actually collect such a detector ?

Undisturbed ambient ? Deflected ? Accelerated or repelled ?

Only Ambient ? No secondaries ?

Modelling Particle Detectors – Top Hat Analyser



Electrostatic analyzer SWA-EAS for Solar Orbiter -
Source : D.O. Kataria - MSSL

Modelling Particle Detectors – Top Hat Analyser

2) Detector calibration

$$f_D \rightarrow f_M$$

1) Electrostatic effects + field of view

$$f_\infty \rightarrow f_D$$

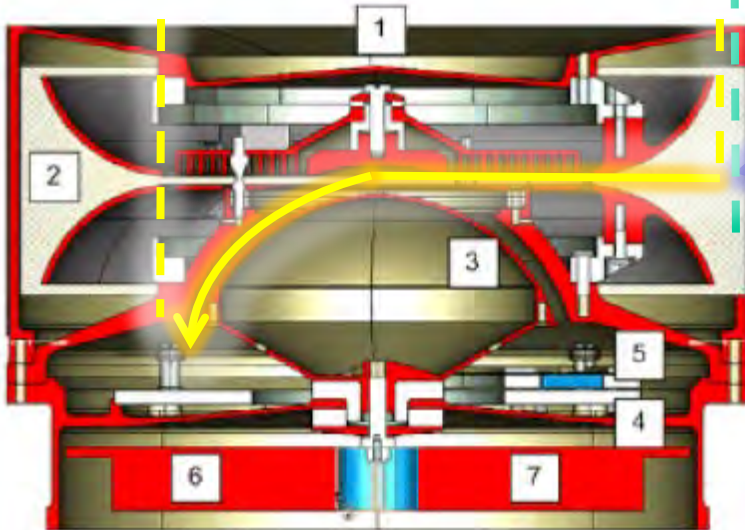
0) Undisturbed plasma

$$f_\infty(V_x, V_y, V_z)$$

Non neutral sheath around $\Phi_D \neq 0$

Disturbance of the environment

Here, we are looking at : $f_\infty \rightarrow f_D$



Analytical Modelling : Liouville's Theorem

- Assuming

- Isotropic f_∞
- All trajectories at detector surface D are filled (comes from undisturbed plasma)
- Non-collisional plasma

- Then

- For any velocity V_D on the detector corresponding to V_∞ at infinite,

$$f_D(V_D) = f_\infty(V_\infty)$$

- Method

- Conservation of total energy

$$V_D = \sqrt{V_\infty^2 - \frac{2q\phi_D}{m}}$$

- Constraint

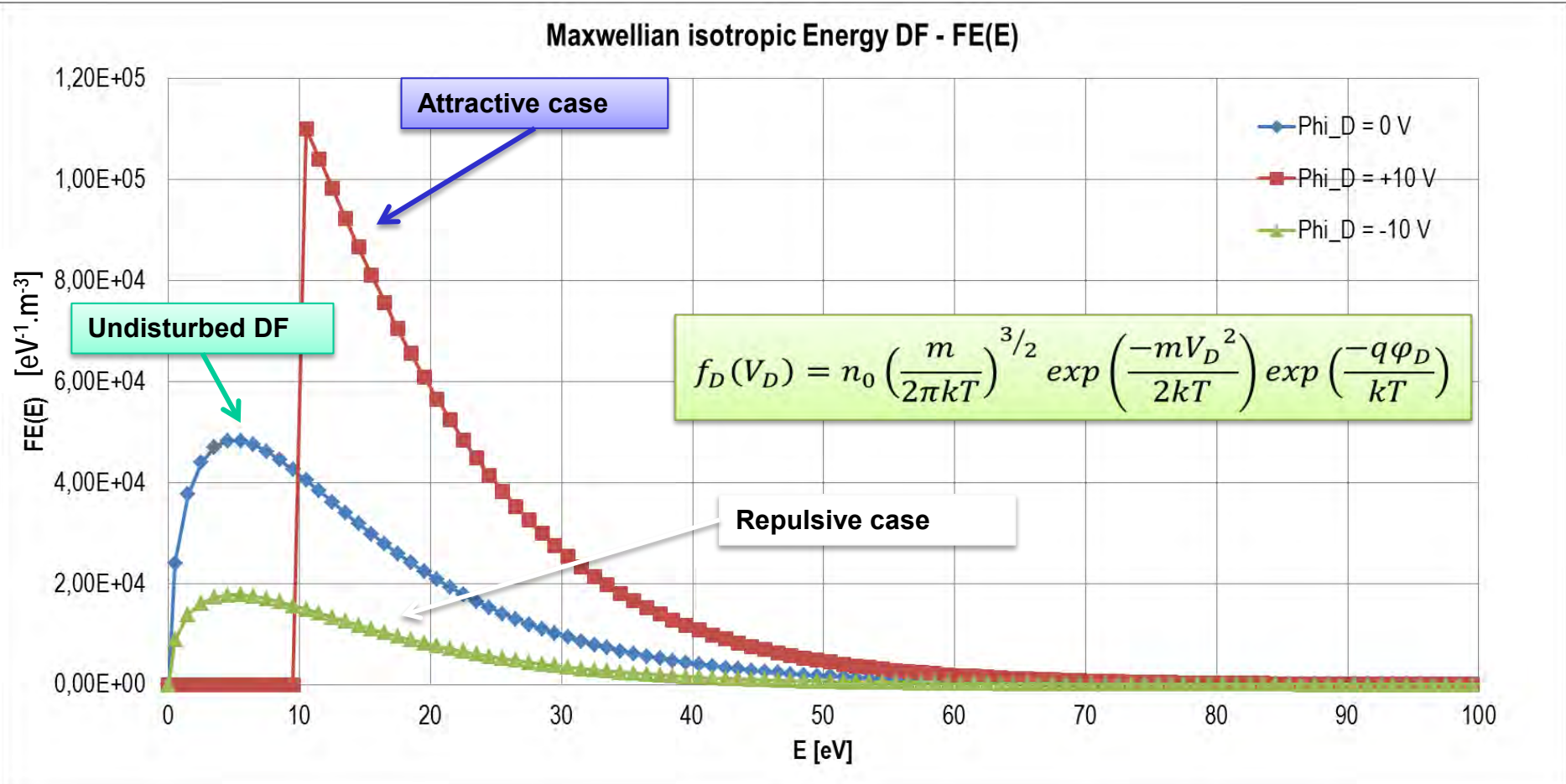
- Positive total energy

$$\frac{1}{2} mV_D^2 + q\phi_D \geq 0$$

Analytical modelling : Liouville's theorem

- Well-known application: Maxwell-Boltzmann distribution

Electrons $kT = 10$ eV



Numerical Modelling with SPIS 5.1

- Assuming
 - Isotropic f_∞
 - All trajectories at detector surface D are filled (comes from undisturbed plasma)
 - Non-collisional plasma

SPIS computes trajectories and tells which ones do really exist

- Then
 - For any velocity V_D on the detector corresponding to V_∞ at infinite,

$$f_D(V_D) = f_\infty(V_\infty)$$

- Method
 - Conservation of total energy

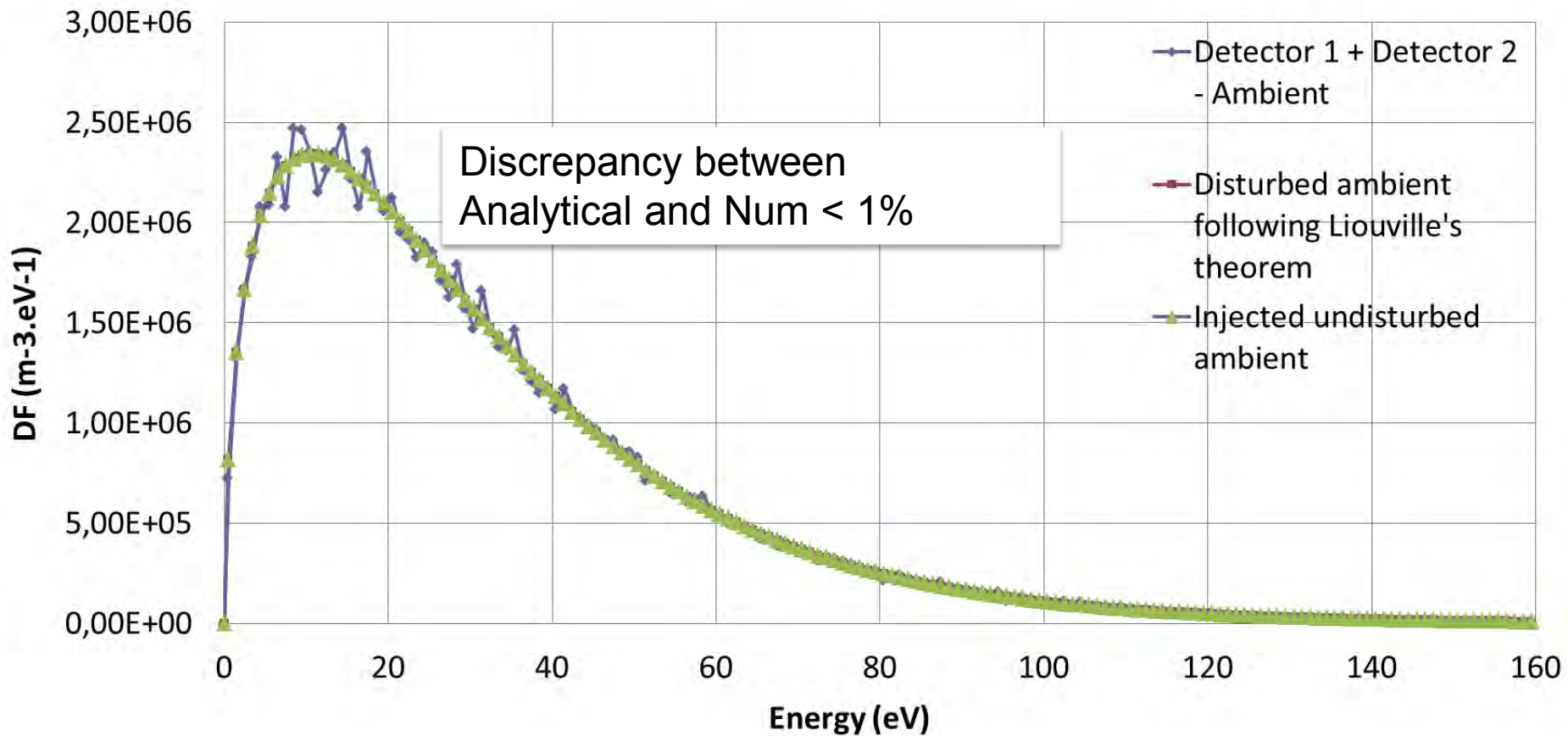
$$V_D = \sqrt{V_\infty^2 - \frac{2q\phi_D}{m}}$$

- Constraint
 - Positive total energy

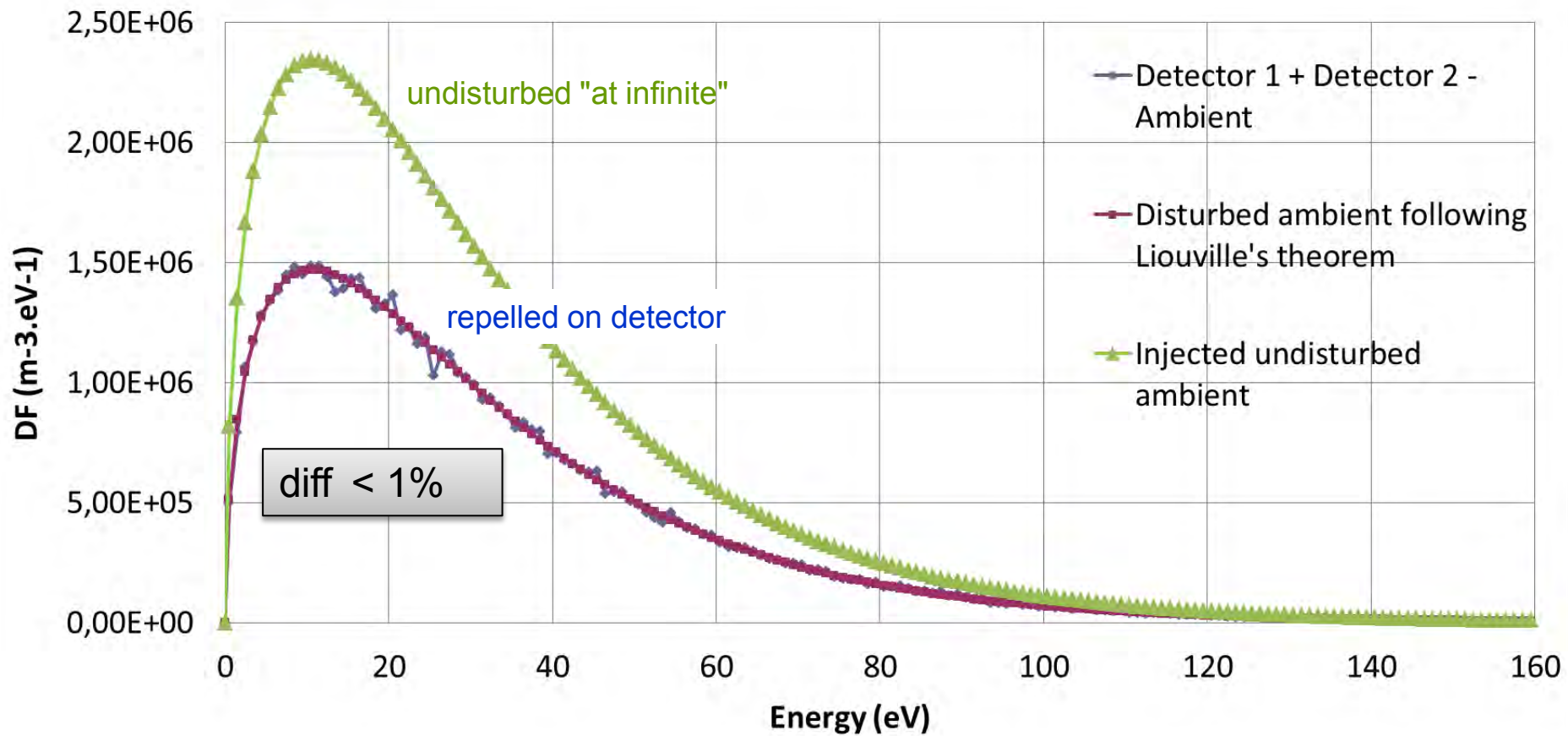
$$\frac{1}{2} m V_D^2 + q\phi_D \geq 0$$

Zero Detector Potential

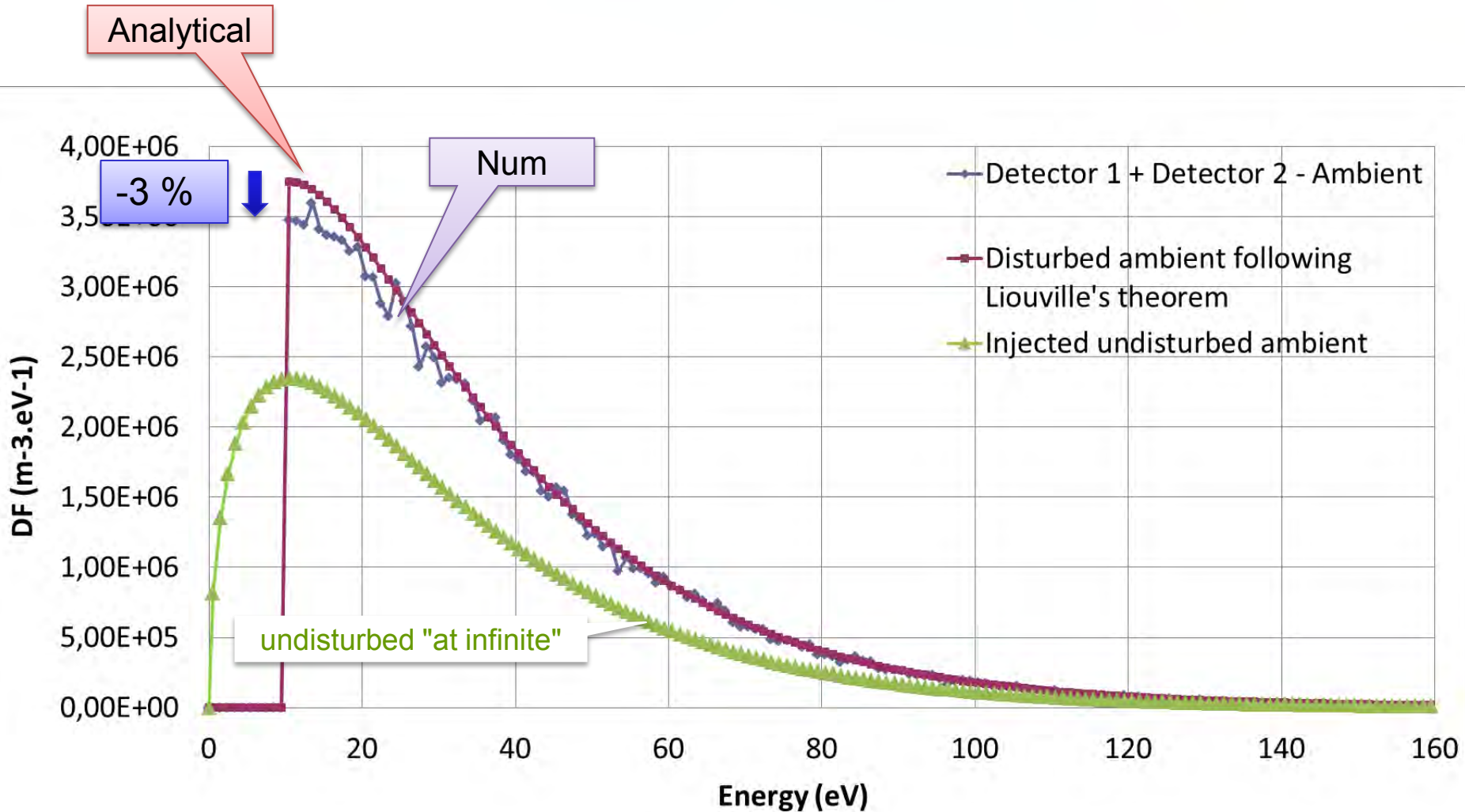
$$\varphi_D = 0 \text{ V}$$



Repulsive Potential -10 V

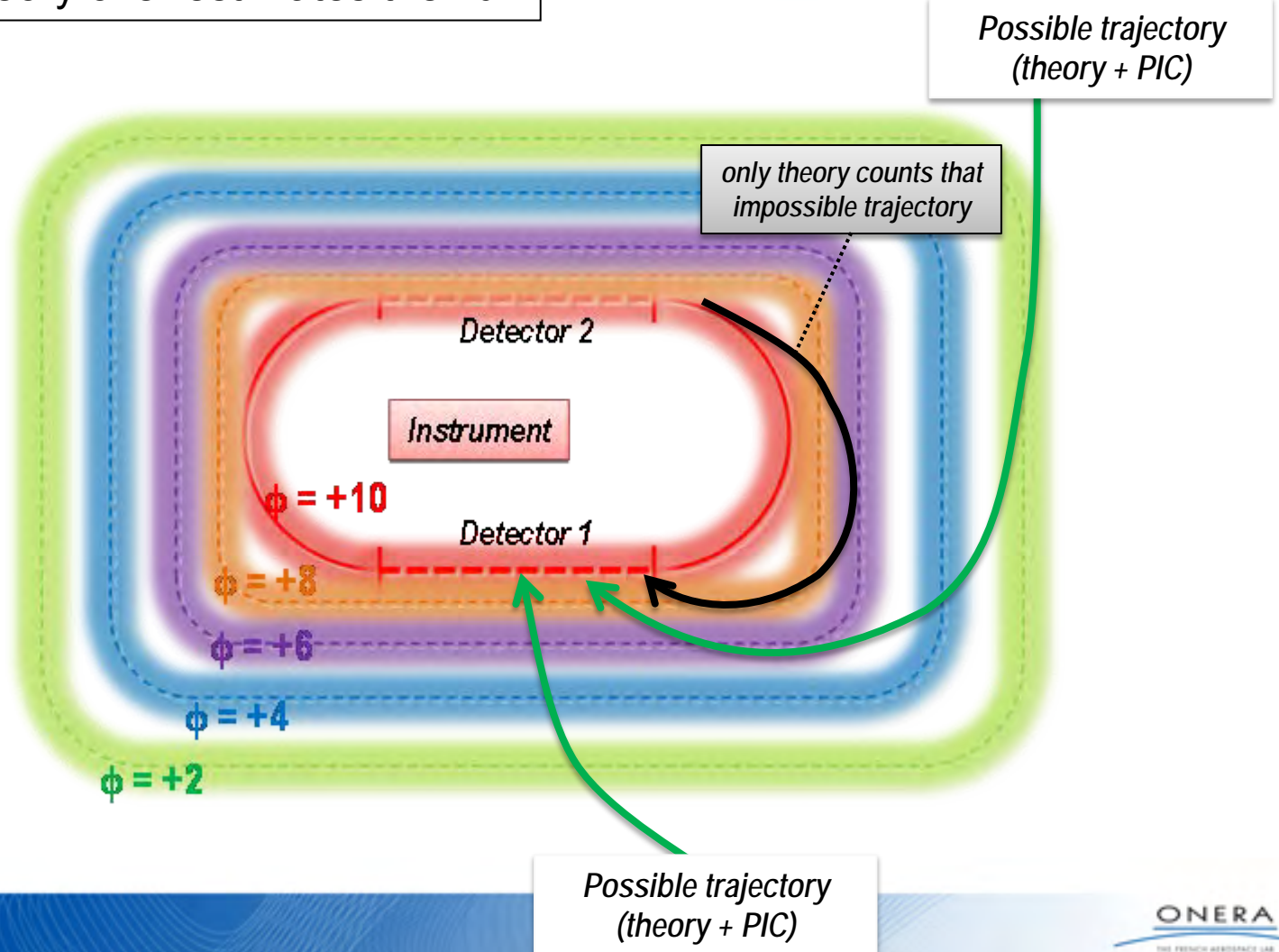


Attractive Potential +10 V



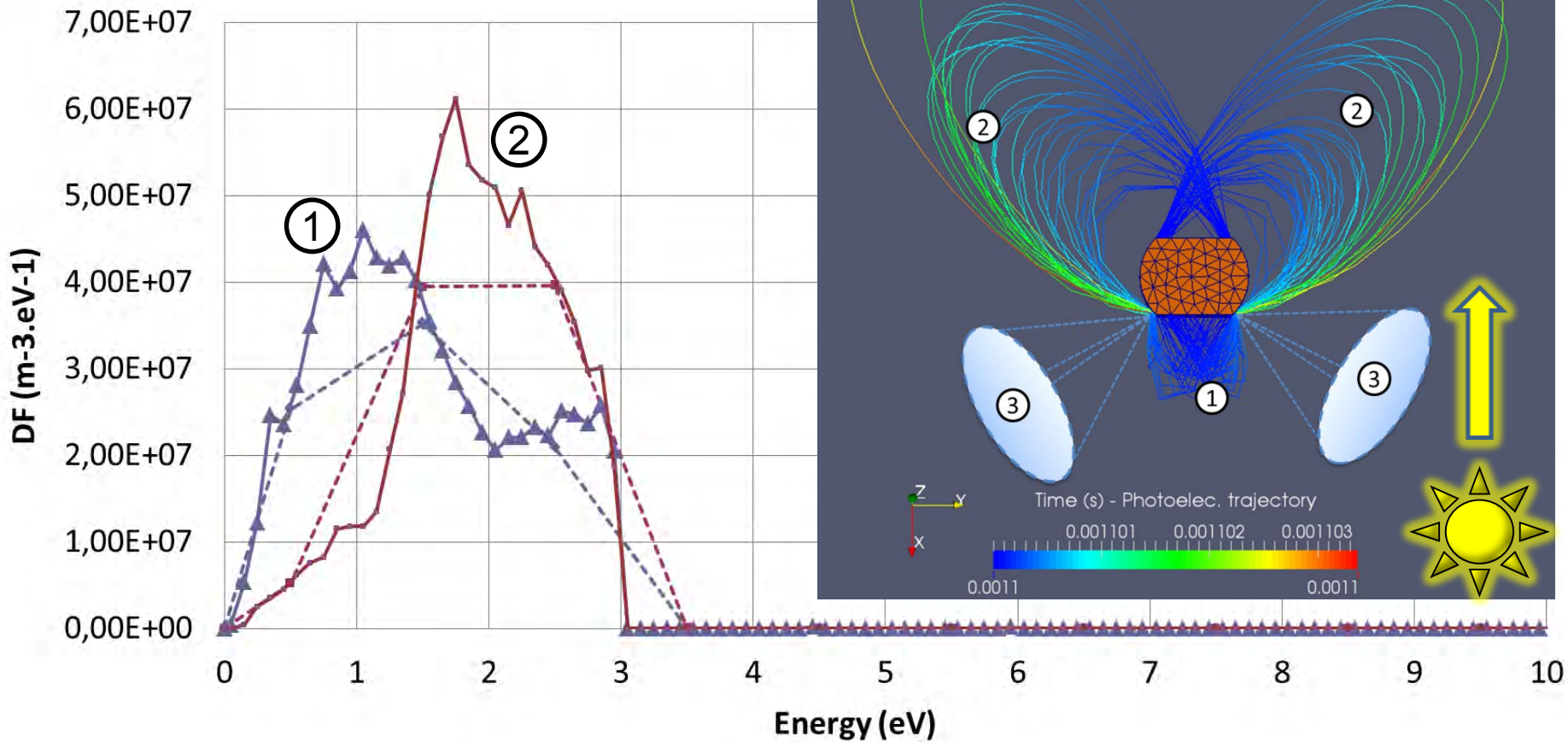
Attractive Potential +10 V

Theory over estimates the flux

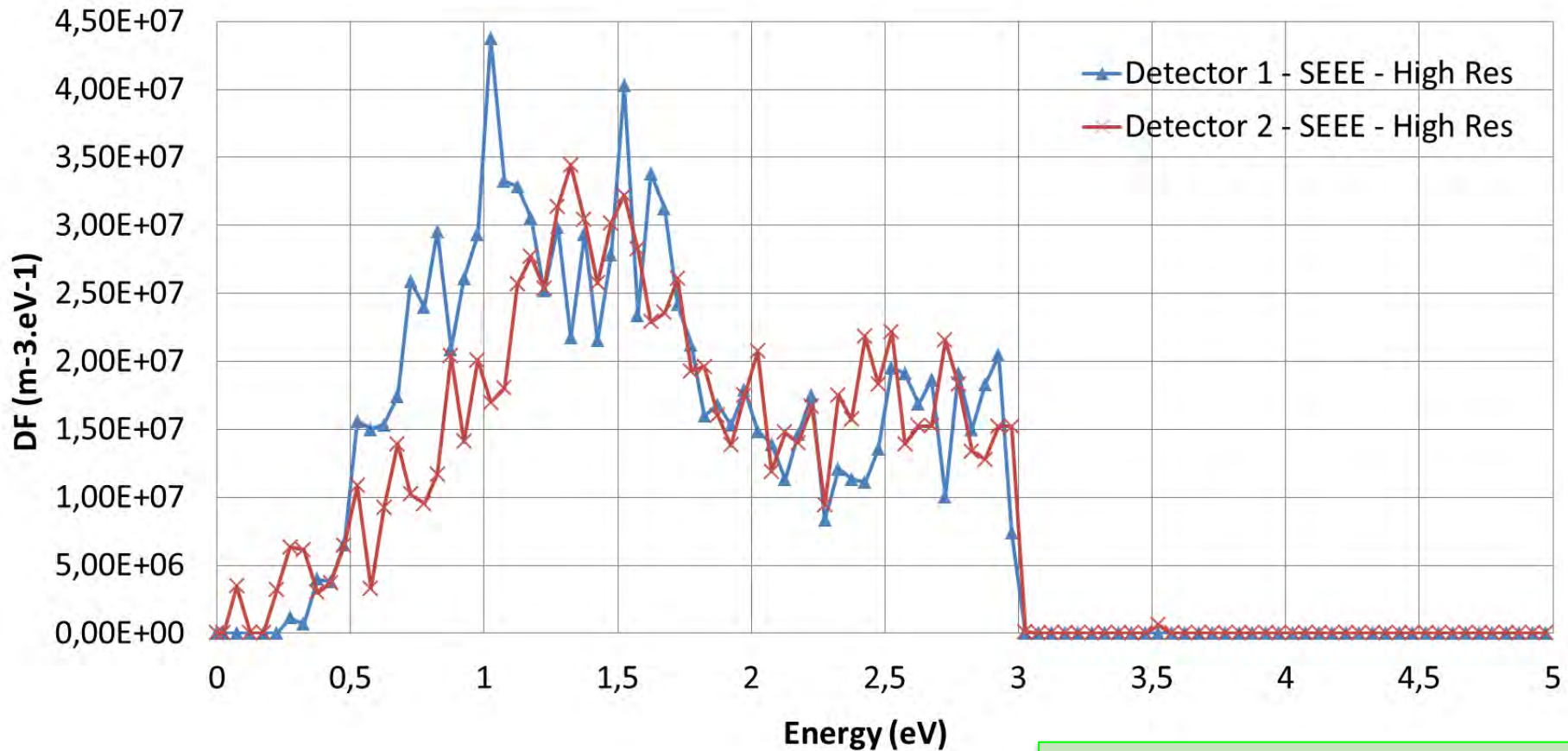


13th SCTC, 23-27/06/2014, Pasadena, CA, USA

Photo Electrons Recollection by Attractive + 3 V



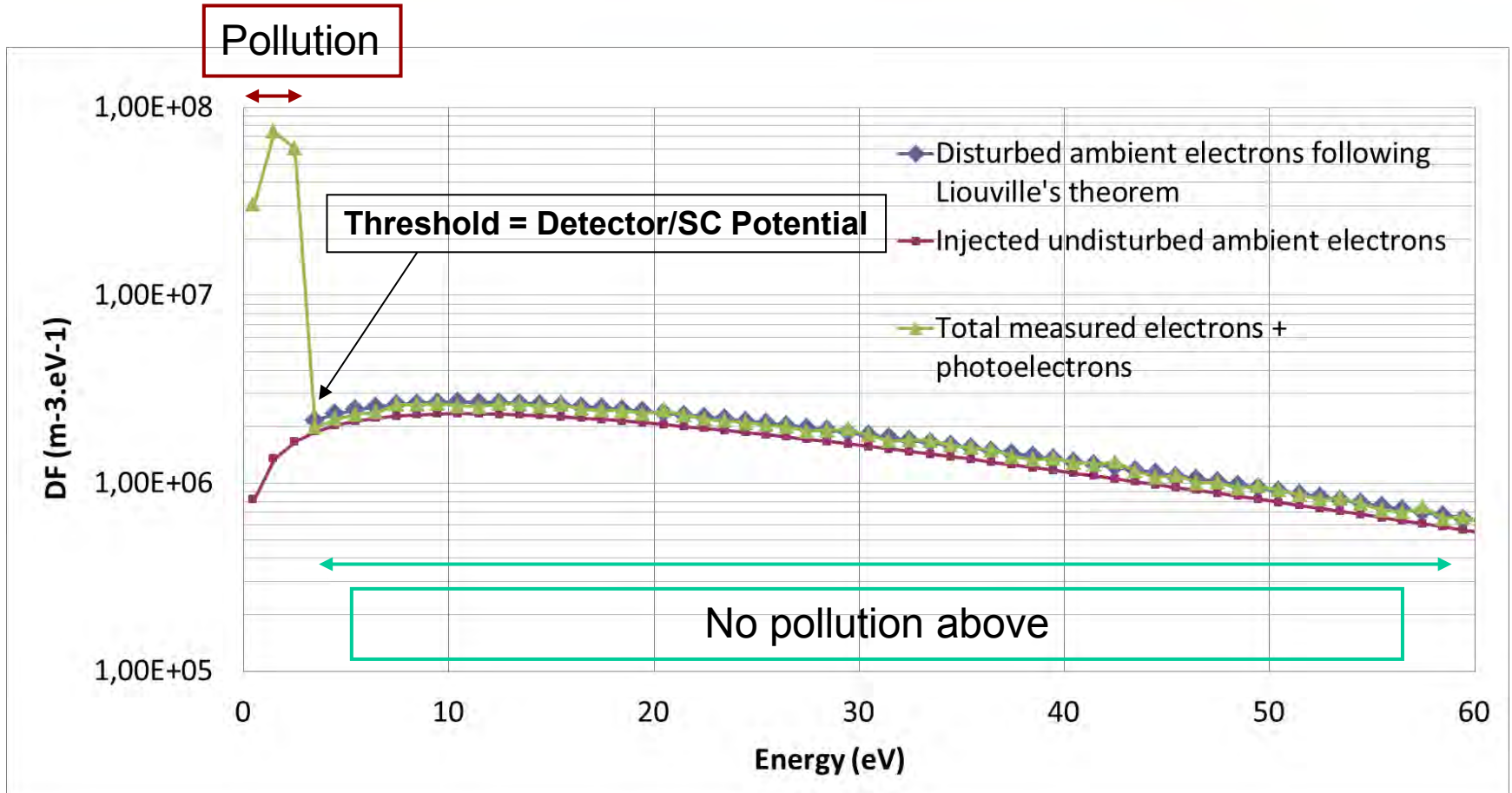
Secondary Electrons under Electron Impact Recollection by attractive +3 V



Re-collection (trapped)

No re-collection
(escape)

Photo Electrons Disturbance



In theory, electron spectra do not mix with each other



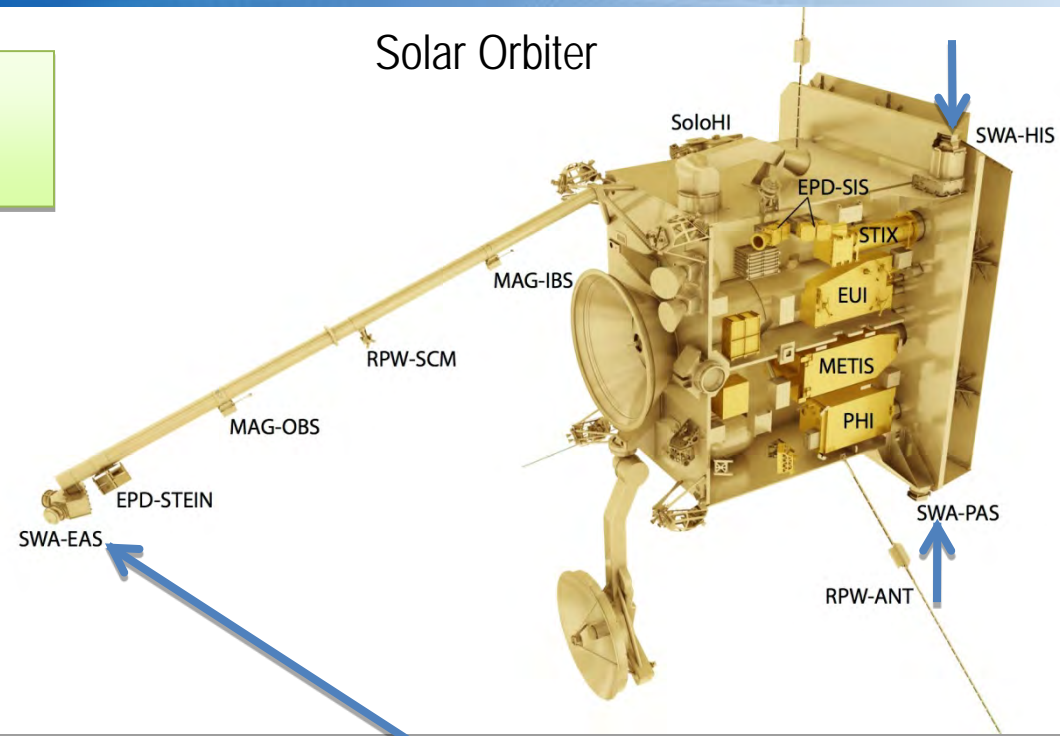
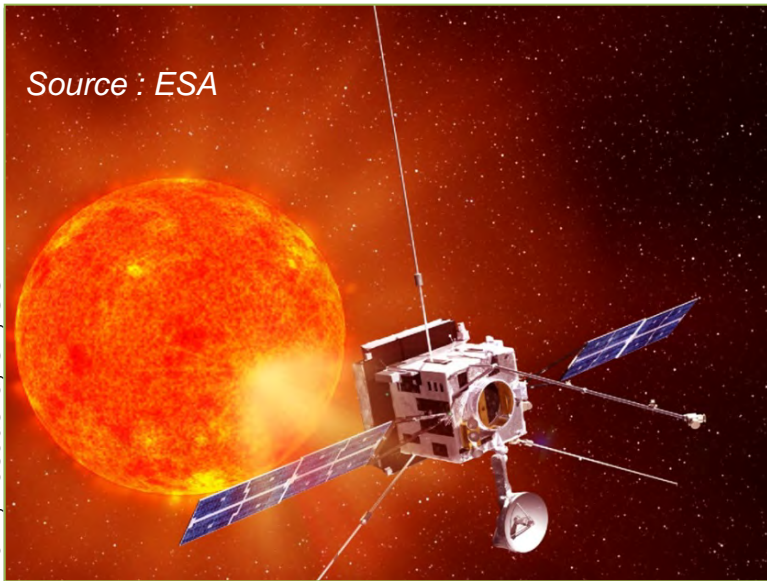
Detector on Solar Orbiter



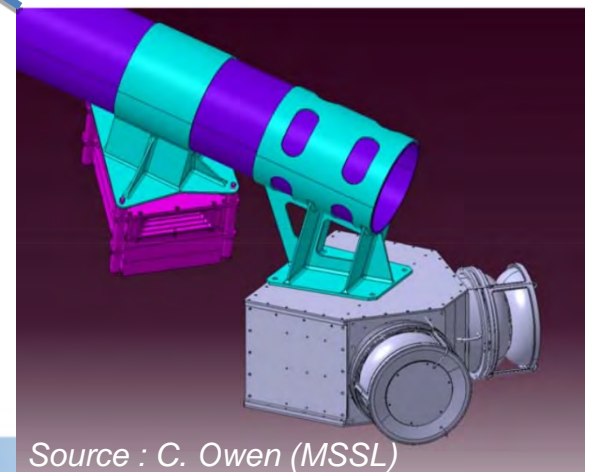
r e t u r n o n i n n o v a t i o n

Solar orbiter

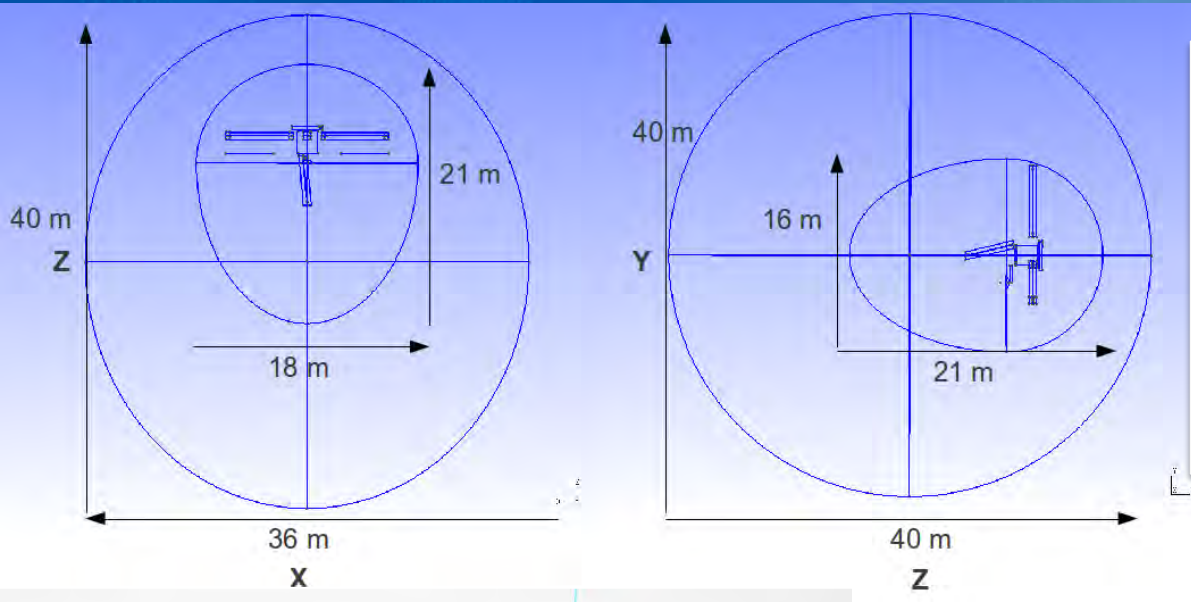
- **ESA** mission : launch 2017 – 2018
- Heliosphere, magnetic field and solar wind
- Orbit : 0.9 to 0.28 AU



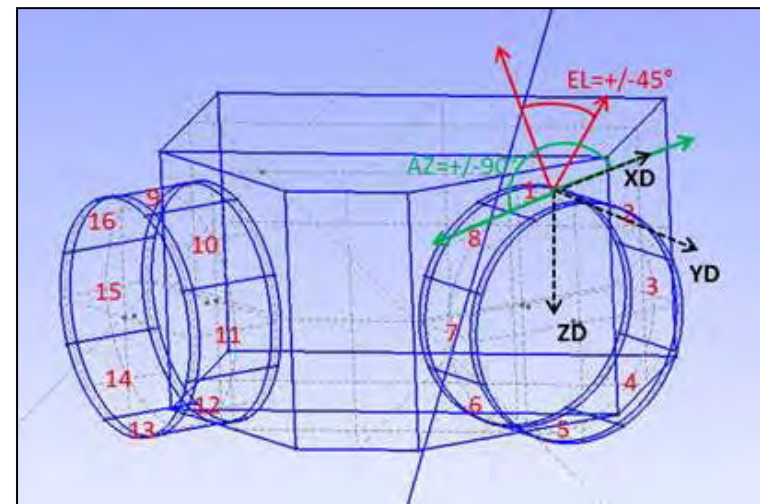
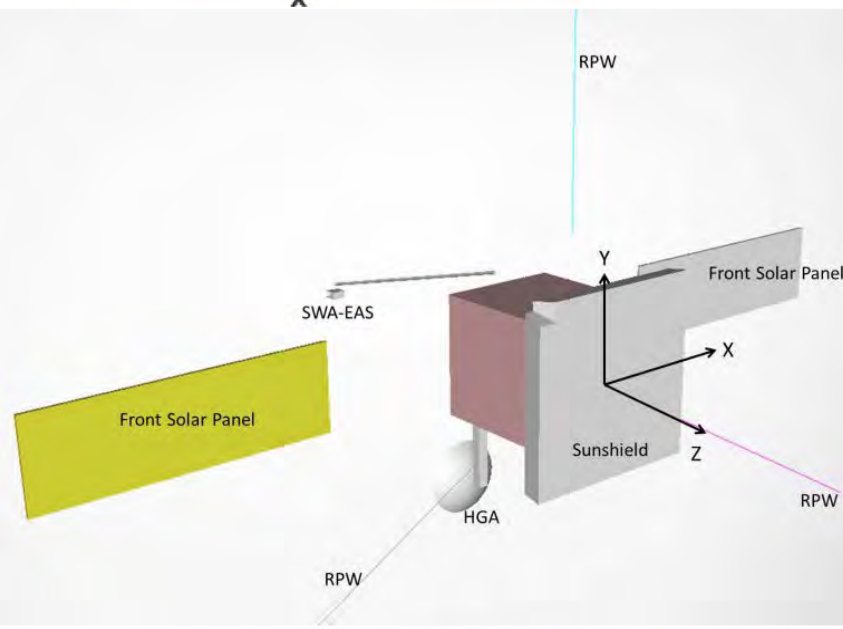
- Instrument group SWA (Solar Wind Analyser)
 - ✓ HIS : Heavy Ion Sensor (IRAP)
 - ✓ PAS : Proton Alpha Sensor (IRAP)
 - ✓ **EAS : Electron Analyser System (MSSL)**



Geometry & mesh



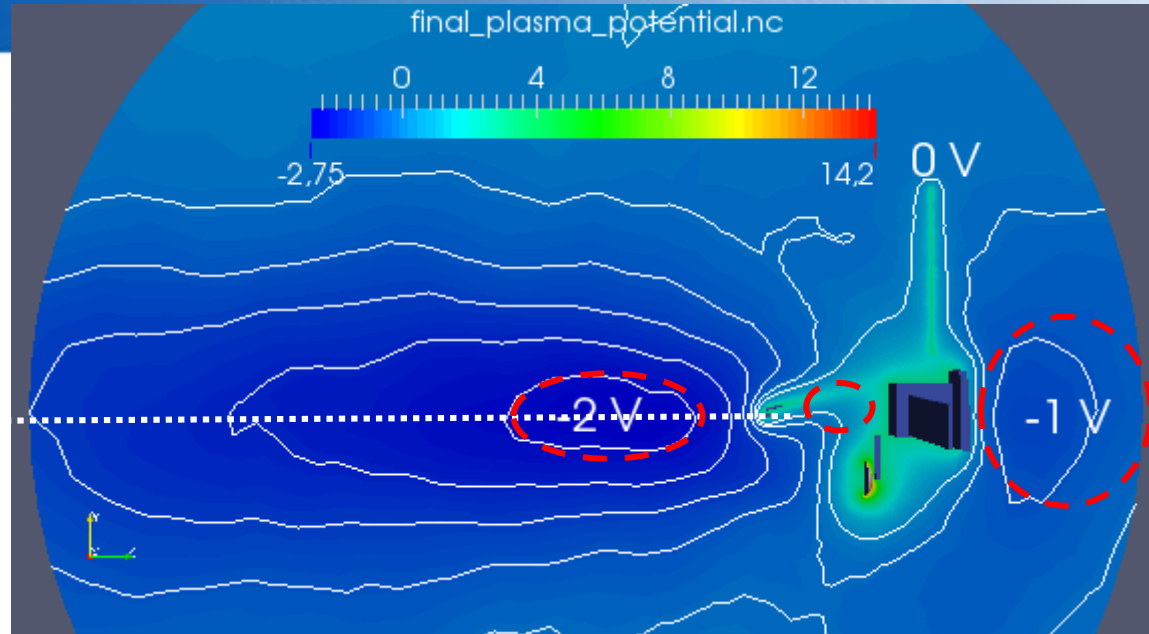
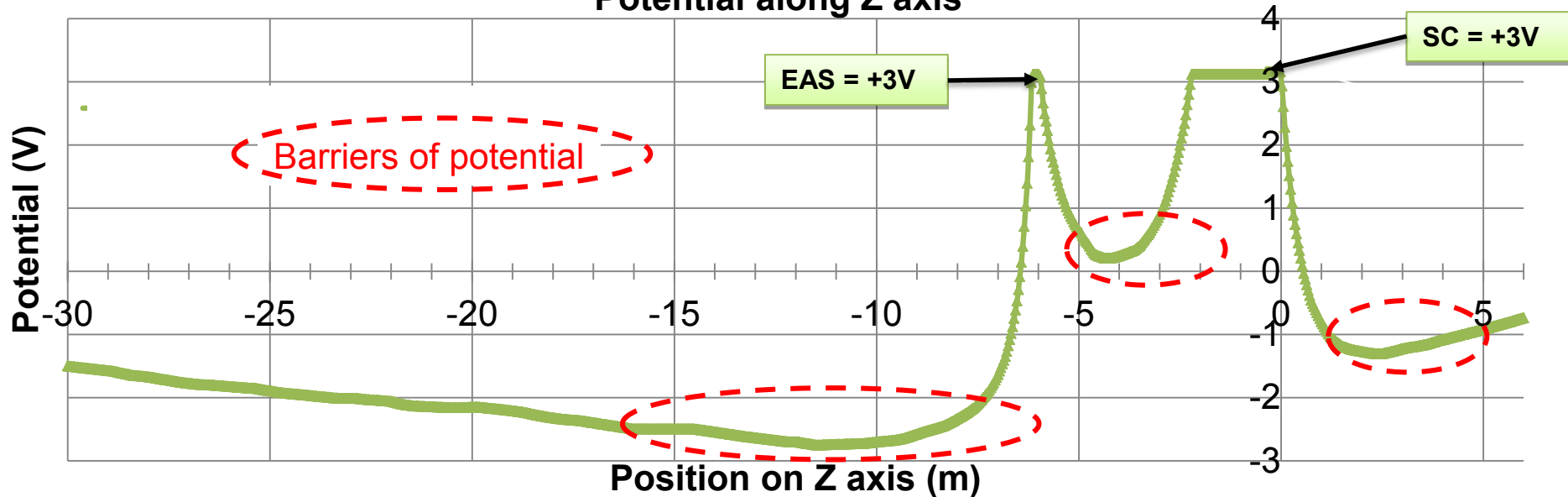
- ✓ Hub : 1.7 x 1.7 x 1.8 m
- ✓ Shield: 2.5 x 2.5 x 0.9 m
- ✓ Solar panels: 3.8 x 1.2 x 0.02 m
- ✓ HGA: 0.5 m
- ✓ EAS on 4 m (long) x 0.02 m (radius) boom
- ✓ 3 RPW antennas (LESIA): 5.3 m (long) x 6 mm (radius)



- Mesh:
- ✓ 5mm to 1.5m
 - ✓ ~ 270,000 tetrahedra

@ 0.28 AU

Simulation ID	SOLO@0.28 AU
Distance (AU)	0.28
Distance (R_s)	60.2
Sun Flux (# 1AU)	12.76
Elec. density N_e (m^{-3})	1.04×10^8
Elec. temp. kT_e (eV)	21.37
Ion density N_i (m^{-3})	1.04×10^8
Ion temp. kT_i (eV)	27.0
Ion ram speed (km/s) V_Z	400
Mach number	7.86
Debye length (m)	3.38
Debye length photo (m)	0.27

**Potential along Z axis**

Ambient electrons

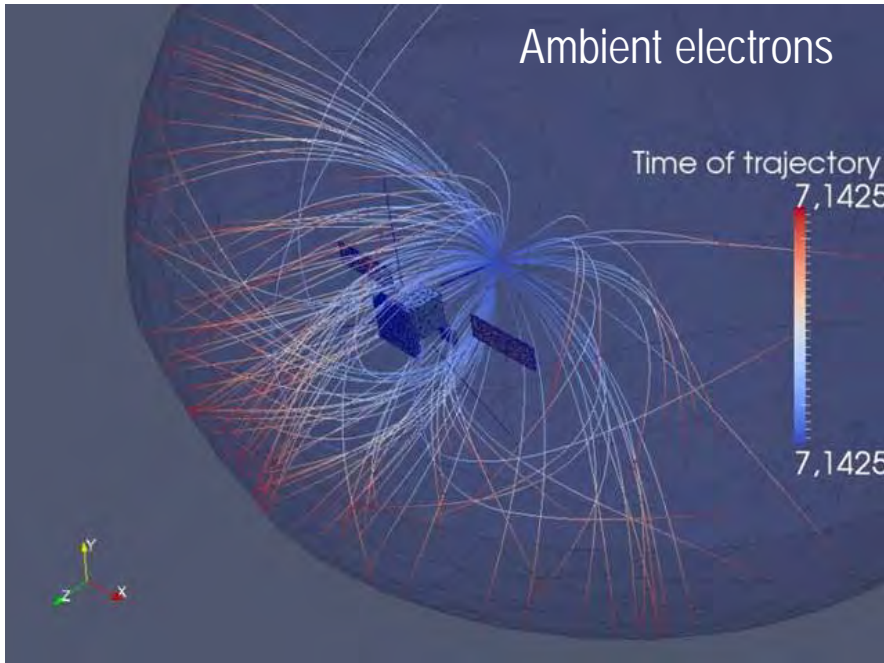
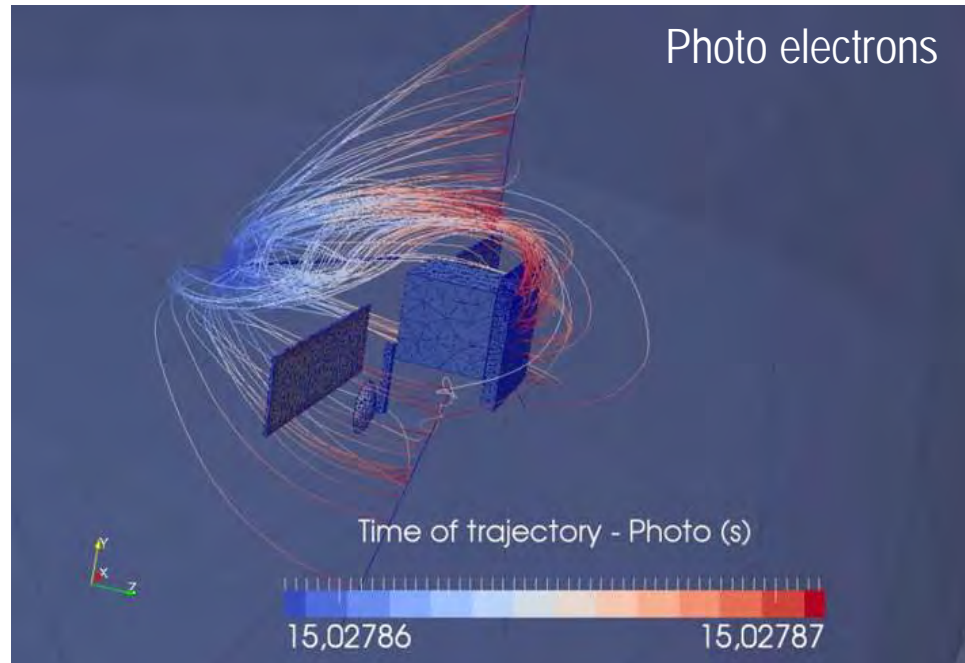
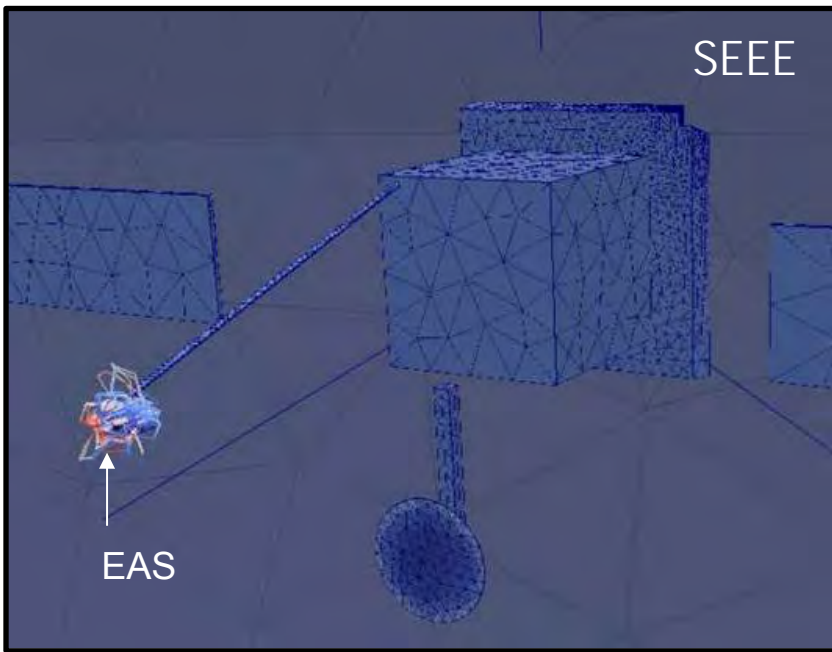


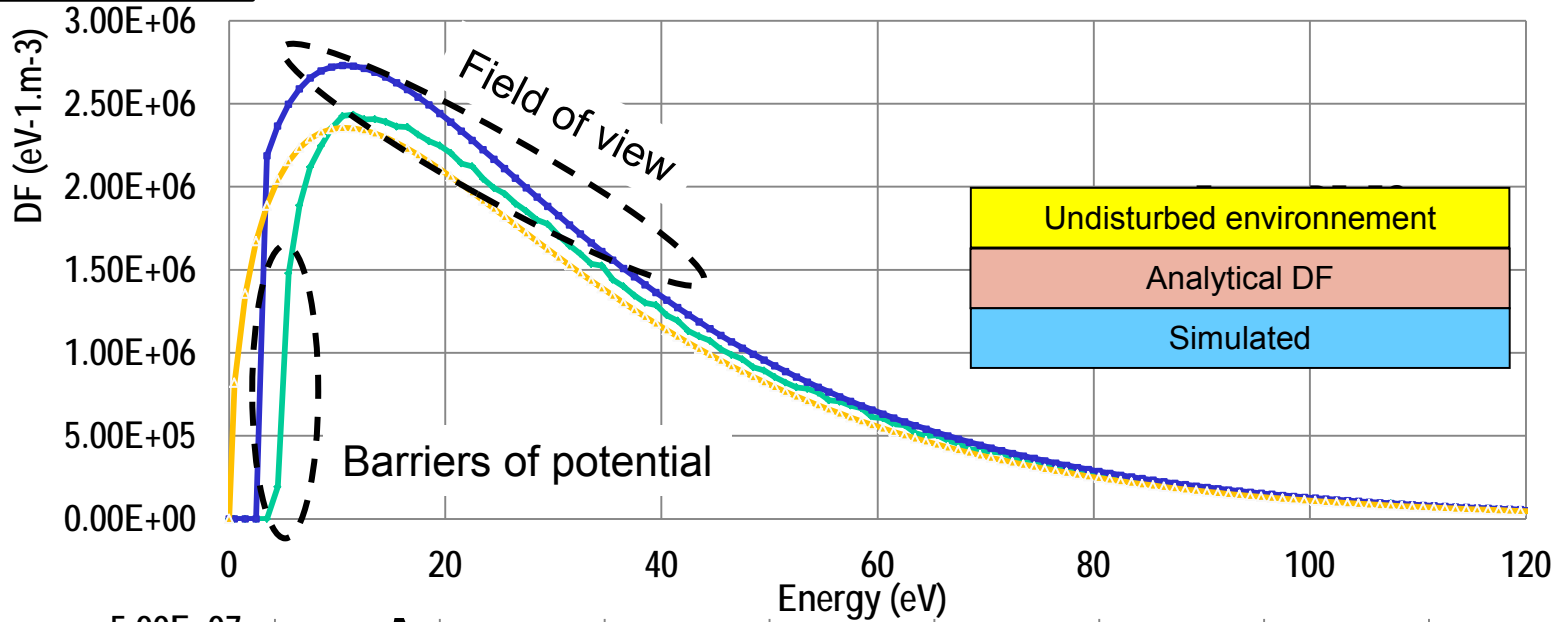
Photo electrons



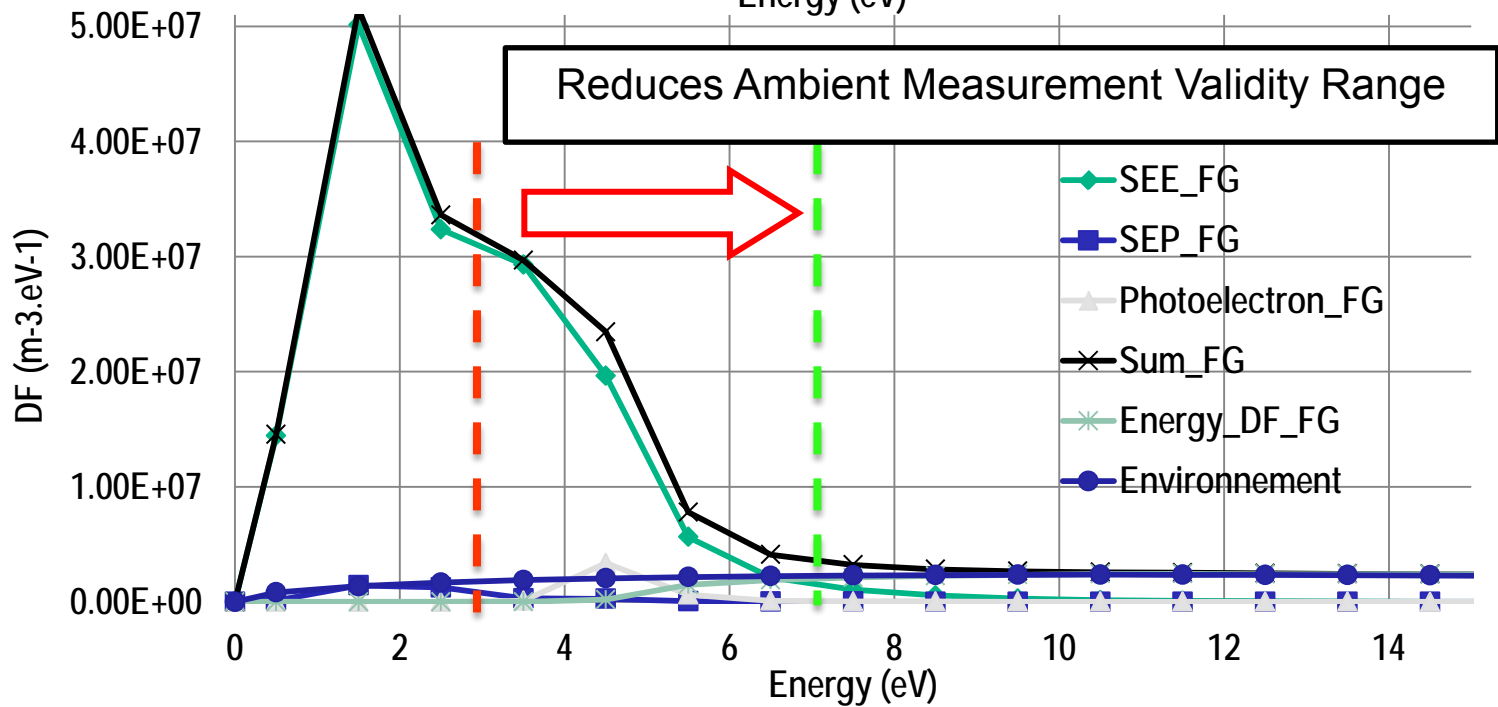
SEEE



Ambient electrons



Secondaries





Summary



r e t u r n o n i n n o v a t i o n

Summary

- Solar orbiter particle instruments have to deal with contamination of **SEEE** electrons coming from the detector itself
- Effect of **photoelectrons** on Cluster → not illustrated, to be submitted for publication
- **SPIS 5** adapted to scientific missions dealing with low energy plasma measurements
- Simulations will permit to
 - Propose means to anticipate disturbance
 - Investigate how measurements can be better understood (and possibly corrected)

Have a look to R. Marchand et al. paper on IAP Journal
Solar Probe Plus simulation with Ptetra, IPIC3D, EMSES, LASP and SPIS

Thanks !

- PhD thesis of Stanislas Guillemant (Feb 2014)
 - Sponsored by CNES and Region Midi-Pyrénées (FR)
 - Supervisors
 - Vincent GÉNOT and Philippe LOUARN (IRAP – GPPS)
 - Jean-Charles MATÉO-VÉLEZ (ONERA – DESP)



- ESA Co ESTEC/4000102091/10/NL/AS
 - SPIS-SCIENCE
 - Technical Officer : Alain Hilgers

- Partners



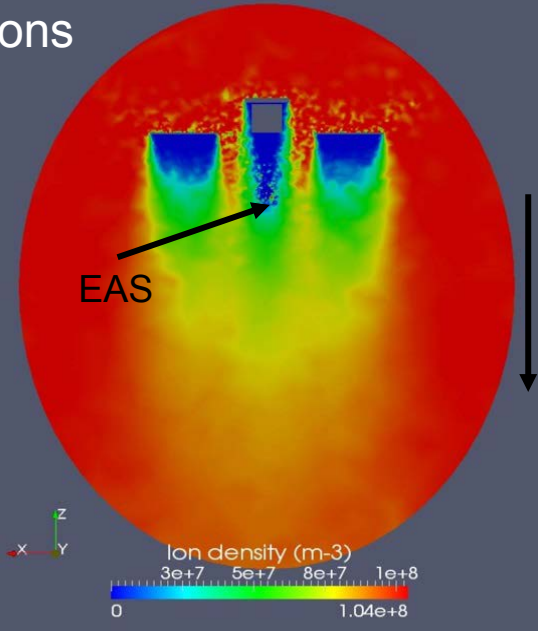


ONERA

THE FRENCH AEROSPACE LAB

r e t u r n o n i n n o v a t i o n

ions



electrons

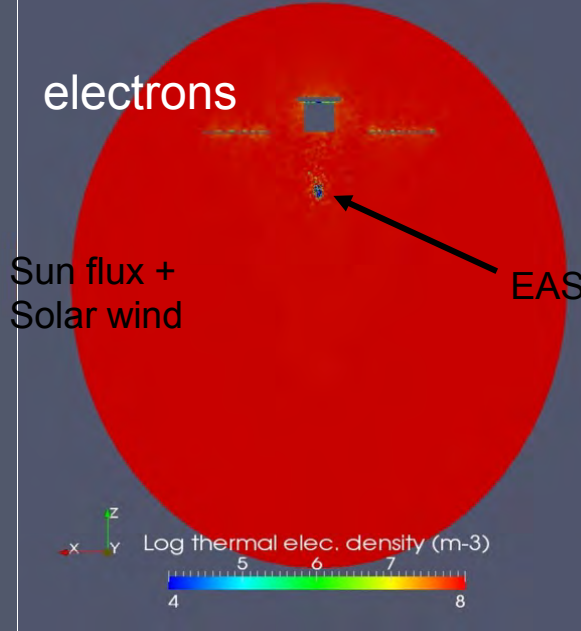
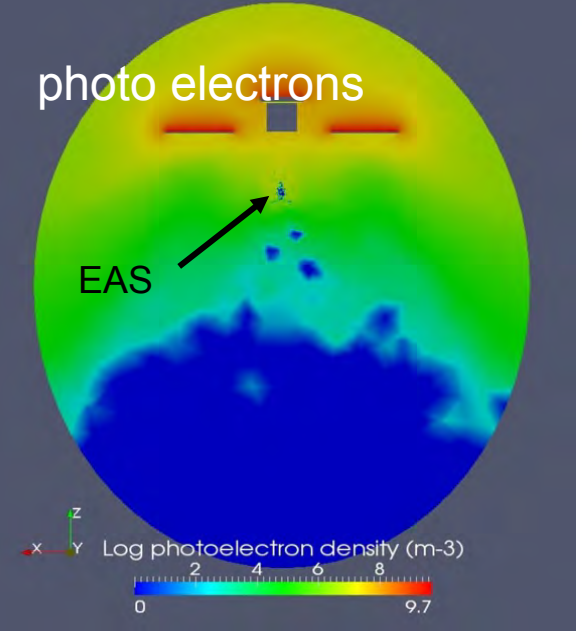
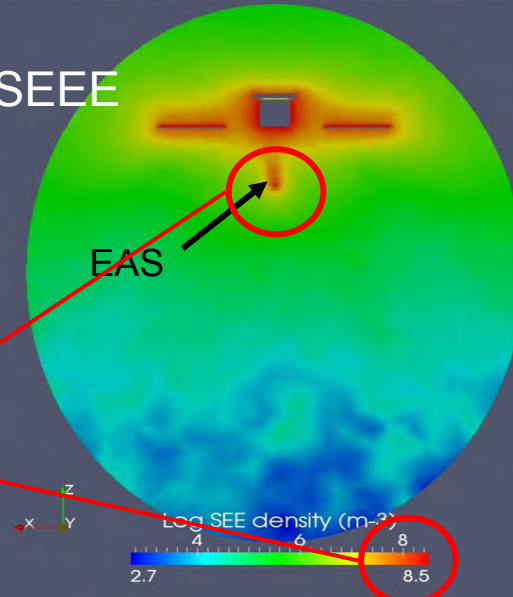


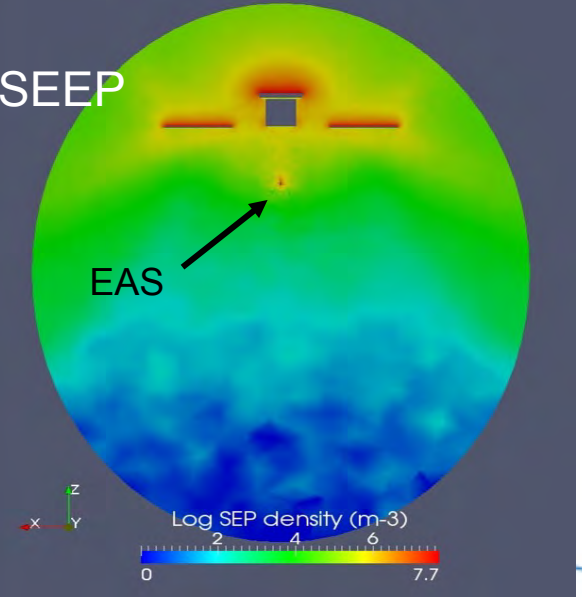
photo electrons



SEEE



SEEP



EAS :

- inside the wake
- surrounded by barriers of potential of -1 to -2 V
- lots of secondary electrons by electron impact

Photo Electrons Recollection by Attractive + 3 V

